CELL BIOLOGY

LncRNA GIRGL drives CAPRIN1-mediated phase separation to suppress glutaminase-1 translation under glutamine deprivation

Ruijie Wang[1]*, Leixi Cao[1]*, Rick Francis Thorne[1,2], Xu Dong Zhang[1,3], Jinming Li[1], Fengmin Shao[1†], Lirong Zhang[1†], Mian Wu[1,4,5†]

Glutamine constitutes an essential source of both carbon and nitrogen for numerous biosynthetic processes. The first and rate-limiting step of glutaminolysis involves the generation of glutamate from glutamine, catalyzed by glutaminase-1 (GLS1). Shortages of glutamine result in reductions in GLS1, but the underlying mechanisms are not fully known. Here, we characterize a long noncoding RNA, GIRGL (glutamine insufficiency regulator of glutaminase lncRNA), that is induced upon glutamine starvation. Manipulating GIRGL revealed a relationship between its expression and the translational suppression of GLS1. Cellular GIRGL levels are balanced by a combination of transactivation by c-JUN together with negative stability regulation via HuR/Ago2. Increased levels of GIRGL in the absence of glutamine drive formation of a complex between dimers of CAPRIN1 and GLS1 mRNA, serving to promote liquid-liquid phase separation of CAPRIN1 and inducing stress granule formation. Suppressing GLS1 mRNA translation enables cancer cells to survive under prolonged glutamine deprivation stress.

INTRODUCTION

Glutamine is the most abundant circulating amino acid (*1*–*2*) and, along with exogenous glucose, represents a major cellular resource for macromolecule synthesis and biomass accumulation. Glutamine metabolites serve as both carbon and nitrogen sources for the biosynthesis of many important cellular components including trichloroacetic acid cycle intermediates, fatty acids, and nucleotides (*3*). Glutamine catabolism is widely exploited by cancer cells, and many cultured in glutamine-deprived medium are unable to proliferate and will eventually die (*4*). Cancer cells exposed to nutrient-deficient conditions may also meet their demand for glutamine through breaking down macromolecules (*5*).

Exogenous glutamine is primarily transported into cancer cells through the alanine-serine-cysteine transporter 2 (ASCT2) (*6*). After uptake and transport into mitochondria, glutamine is converted to glutamate, which is further catabolized through glutamate dehydrogenase (GDH) or transaminases [glutamic pyruvic transaminase (GPT)/glutamic oxaloacetic transaminase (GOT)], coupled with production of NADH (reduced form of nicotinamide adenine dinucleotide), NADPH [reduced form of nicotinamide adenine dinucleotide phosphate ($NADP^+$)], ammonium, and other nonessential amino acids (NEAAs) (*7*). Moreover, glutamine is an important substrate for the synthesis of a key intracellular antioxidant glutathione. Glutathione is a tripeptide (Glu-Cys-Gly), which serves to neutralize peroxide free radicals and mediates ROS (reactive oxygen species) homeostasis through production of NADPH via glutamate dehydrogenase 1 (GLUD1) (*8*–*9*).

Glutamine conversion to glutamate is catalyzed by mitochondrial glutaminase (GA), an enzyme encoded by two genes in mammals, namely, the kidney-type (GLS1) and liver-type (GLS2) glutaminases (*10*). The expression of GLS2 is restricted to certain normal tissue types, whereas GLS1 is more broadly expressed among normal tissues and thought to largely contribute to the aberrations in glutamine catabolism observed in cancer cells (*11*). Notably, GLS1 is frequently overexpressed in numerous malignant tumors and acts as an oncogene to support cancer growth (*12*–*13*). In contrast, silencing of GLS2 by promoter methylation occurs in glioblastoma, liver, and colorectal cancers, and its reexpression suggests it functions as a tumor suppressor (*14*–*15*). Alternative splicing of GLS1 adds further complexity, with the glutaminase C (GAC) isoform exhibiting higher enzymatic activity compared to the kidney-type glutaminase (KGA) isoform (*16*–*17*). Of relevance to this report, GLS1 expression can decrease under conditions of glutamine deprivation (*18*), although the underlying mechanism remains unclear.

Long noncoding RNAs (lncRNAs) are defined as non–protein-coding RNA transcripts longer than 200 nucleotides (*19*). They exhibit controls over both gene and protein expression and function through an extensive repertoire of mechanisms, including chromatin modification and transcriptional and posttranscriptional events along with protein interactions (*20*–*21*). Dysregulation of lncRNAs has been linked to a variety of human cancers (*22*), with several examples of lncRNAs known to be involved in the regulation of glutamine metabolism. For example, the lncRNA ACOD1 enhances the catalytic activity of glutamic-oxaloacetic transaminase through direct binding near its substrate niche (*23*). With respect to GLS1, the lncRNA GLS-AS targets and down-regulates GLS1 mRNA at the posttranscriptional level via an ADAR/Dicer-dependent RNA interference mechanism (*24*). In addition, lncRNA-CCAT2 regulates the alternative splicing of GLS1 in colorectal cancer, resulting in the preferential expression of the more catalytically active isoform GAC over KGA (*25*).

[1]Translational Research Institute, Henan Provincial People's Hospital, Academy of Medical Science, Zhengzhou University, Zhengzhou 450053, China. [2]School of Environmental and Life Sciences, University of Newcastle, Callaghan, NSW 2258, Australia. [3]School of Biomedical Sciences and Pharmacy, University of Newcastle, Callaghan, NSW 2308, Australia. [4]School of Clinical Medicine, Henan University, Zhengzhou 450003, China. [5]CAS Key Laboratory of Innate Immunity and Chronic Disease, CAS Centre for Excellence in Molecular Cell Science, The First Affiliated Hospital of University of Science and Technology of China, Hefei 230027, China.
*These authors contributed equally to this work.
†Corresponding author. Email: fengminshao@126.com (F.S.); lrzhang@zzu.edu.cn (L.Z.); wumian@ustc.edu.cn (M.W.)

Here, we demonstrate that an lncRNA we call GIRGL is induced via metabolic stress responses elicited by c-Jun. GIRGL functions to attenuate GLS1 expression in cells deprived of glutamine. Under basal conditions, the levels of GIRGL are restrained via the activity of the RNA binding protein HuR (human antigen R), known for stabilizing mRNAs or modulating their translation (*26*–*27*). HuR affects GIRGL transcript stability via an Ago2-mediated RNA-induced silencing complex (RISC) mechanism, consistent with recent findings showing that HuR can suppress mRNA targets such as c-Myc mRNA and lincRNA-p21 by facilitating interactions with let-7/RISC (*28*–*29*). In cells deprived of glutamine, the elevated levels of GIRGL function to inhibit GLS1 translation by acting as a scaffold that facilitates the dimerization and activation of CAPRIN1 (*30*). CAPRIN1 is a ubiquitously expressed cytosolic phosphoprotein (*31*) variously involved in stress responses (*32*) and mRNA localization/stability (*30*, *33*) and is both an agonist and an antagonist of translational activity (*34*–*35*). CAPRIN1 has also been shown to facilitate stress granule (SG) formation, membrane-less organelles arising by liquid-liquid phase separation (*36*), and this subcompartmentalization process has recently been implicated in regulating translation (*34*). We show here that glutamine deprivation causes GIRGL, CAPRIN1, and GLS1 mRNA to redistribute to SGs and, moreover, demonstrate that GIRGL itself promotes CAPRIN1-dependent phase separation. Manipulating GIRGL in cancer cells demonstrated that its expression is antiproliferative under glutamine-replete conditions but allowed cells to survive in the absence of glutamine, indicative of a role in adaptive responses to nutrient stress.

RESULTS

LncRNA GIRGL negatively regulates cellular glutamine metabolism through suppression of GLS1

We hypothesized that lncRNAs induced in response to glutamine deprivation would be involved in metabolic adaptation including the down-regulation of glutaminases (*18*). Of the two glutaminase isoforms GLS1 and GLS2, we need to ascertain whether they are both down-regulated in the absence of glutamine. We first established that GLS1, but not GLS2, protein levels decreased in a time-dependent manner during glutamine starvation in HCT116 cells (fig. S1A). The HCT116 model system was then subjected to microarray analyses to identify candidate lncRNAs induced during glutamine deprivation (table S1). From these data, 14 responsive lncRNAs were validated by quantitative polymerase chain reaction (qPCR) along with the previously characterized c-Myc gene (fig. S1B). This screen produced a total of six lncRNAs whose expression was significantly elevated in response to glutamine starvation. Each of the lncRNAs (Gln-1, Gln-4, Gln-6, Gln-7, Gln-12, and Gln-14) was then depleted in HCT116 cells using two independent short hairpin RNAs (shRNAs), with the efficacy of knockdown confirmed by qPCR. Among these, silencing of Gln-4 (ENSG00000233834.2, LOC100506098), but not other lncRNAs, resulted in increased GLS1 protein levels relative to shRNA control–treated cells (fig. S1C). On this basis, we focused our subsequent investigations on Gln-4, which we name GIRGL (glutamine insufficiency regulator of glutaminase lncRNA).

Supplementing the findings of the shRNA experiments, overexpression of GIRGL in HCT116 cells decreased the expression of GLS1 (Fig. 1A). Moreover, the introduction of an shRNA-resistant GIRGL construct (GIRGL-R) in shGIRGL-treated cells restored the expression of GLS1 (Fig. 1B), thus ruling out that the actions of GIRGL on GLS1 expression resulted from off-target effects. Extending our analyses to a second colorectal carcinoma cell line, HT29, confirmed that knockdown of GIRGL increases GLS1 levels, whereas its forced expression decreases GLS1 (Fig. 1, C and D, respectively). Mirroring the changes in GLS1 expression, there were decreased levels of cellular glutaminase activity observed following glutamine deprivation, and furthermore, knockdown of GIRGL resulted in relative increases in glutaminase activity under both glutamine-replete and glutamine-deprived conditions (Fig. 1E). Instructively, knockdown of GLS1 substantially diminished glutaminase activity to the same basal levels in cells cultured with and without glutamine (fig. S1D). In contrast, knockdown of GLS2 had little, if any, effect on cellular glutaminase activity cultured with and without glutamine (fig. S1E), indicating that GLS1 is the major contributor to cellular glutaminase activity.

While GIRGL was strongly induced in a time-dependent manner in both HCT116 and HT29 cells following glutamine starvation, GIRGL levels were unresponsive in NCM460 normal colonic cells (fig. S1F). In addition, the induction of GIRGL was dependent on the glutamine concentration, with maximal induction and effects on GLS1 occurring in the absence of glutamine (fig. S1G). Absolute quantitation of GIRGL levels showed that its basal expression was approximately 30 copies per cell, which increased five- to sixfold upon glutamine starvation (fig. S1H). Moreover, cellular fractionation and imaging by fluorescence in situ hybridization (FISH) showed that GIRGL was substantially localized in the cytoplasm (fig. S1, I and J). Last, we considered the possibility that GIRGL was translated as occurs with some lncRNAs. We identified an internal ribosome entry site (IRES) in GIRGL, albeit with a low probability score (nucleotides 10 to 43), but testing this region using a split green fluorescent protein (GFP) reporter showed no translation, indicating that GIRGL is a bona fide lncRNA (fig. S1K) (*37*). In the context of colon carcinoma cells, these data collectively demonstrate that GIRGL is responsive to the exogenous concentration of glutamine and time of glutamine deprivation, and its induction serves to inhibit GLS1 expression.

From the aforementioned findings, the implied actions of GIRGL on GLS1 would elicit changes in glutamine metabolism. Examining glutamine utilization along with the levels of key metabolites following knockdown of GIRGL in HCT116 cells revealed significantly increased α-KG along with increased levels of glutamine consumption, adenosine 5′-triphosphate (ATP), and NADPH (Fig. 1F and fig. S1, L to N). Furthermore, knockdown of GIRGL led to the down-regulation of intracellular ROS levels (Fig. 1G), consistent with anticipated effects of increased glutathione levels (Fig. 1H) together with accompanying increases in α-KGDH activity (fig. S1O). Next, we measured the oxygen consumption rate (OCR) often used as proxy measure of mitochondrial respiration. Comparing control shRNA cells with those treated with independent shRNAs targeting GIRGL revealed significant increases in OCR, while conversely, ectopically expressed GIRGL significantly decreased OCR (fig. S1, P and Q, respectively). Thus, manipulating GIRGL results in wholesale effects on cell respiration, which is reflected in the observed changes in glutamine metabolites.

We next extended our analysis to investigate the actions of GIRGL on other glutamine-dependent cellular processes. Evaluation of protein synthesis rates showed that GIRGL depletion promoted protein synthesis under both normal and glutamine starvation

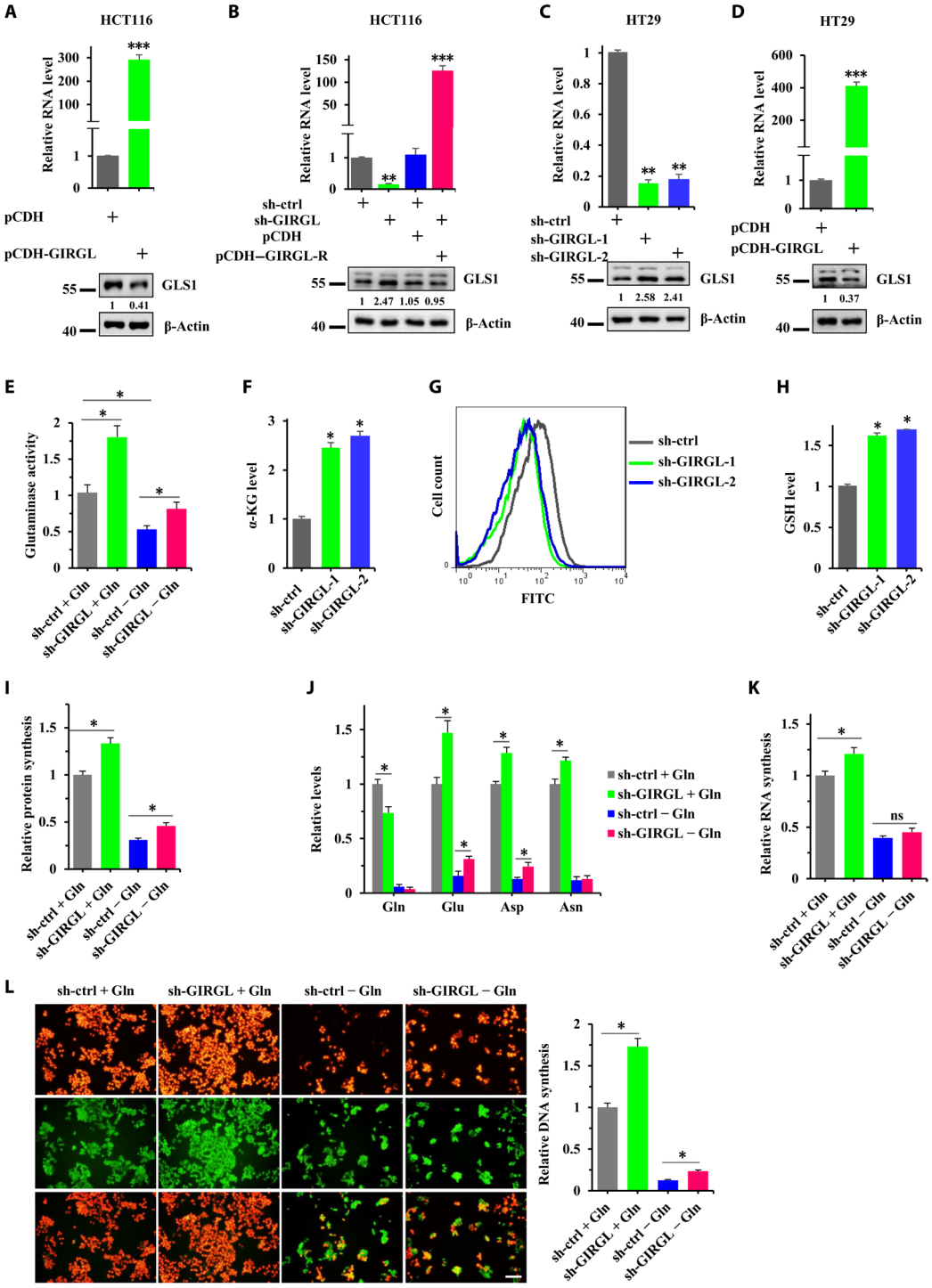

Fig. 1. GIRGL negatively regulates cellular glutamine metabolism. (**A**) Expression of GIRGL (qPCR, top) and GLS1 (Western blot, bottom) in HCT116 cells transduced with control (PCDH) or GIRGL-containing (PCDH-GIRGL) vectors. Relative GLS1 levels were determined throughout by densitometry against the β-actin loading control. (**B**) Expression of GLS1 following shRNA-mediated silencing of GIRGL alone or in combination with an shRNA-resistant GIRGL (GIRGL-R) construct. (**C** and **D**) GLS1 expression in HT29 cells following silencing of GIRGL using two independent shRNAs (sh-1 and sh-2) (C) or following GIRGL overexpression (D). (**E**) Intracellular glutaminase activity in HCT116 cells transduced with shCtrl or shRNAs targeting GIRGL after culture with or without 2 mM glutamine for 24 hours. (**F** to **H**) Cellular α-KG levels (F), ROS levels (G), and GSH levels (H) in HCT116 cells transduced with shCtrl or independent shRNAs targeting GIRGL (sh-1 and sh-2). (**I**) Protein synthesis in HCT116 cells transduced with shCtrl or shRNAs targeting GIRGL cultured with or without 2 mM glutamine for 24 hours. FITC, fluorescein isothiocyanate. (**J**) Intracellular glutamine, glutamate, aspartate, and asparagine levels in HCT116 cells as per (I). (**K**) RNA synthesis in HCT116 cells as per (I). (**L**) DNA synthesis in HCT116 cells as per (I). Epifluorescence microscopy compares de novo DNA synthesis (EdU; red) versus total (green). Representative fields (left) and quantitation (right). (A) to (F) and (H) to (L) are mean ± SD; $n = 3$ independent experiments, two-tailed Student's t test. (G) represents three independent experiments (ns, not significant; $^*P < 0.05$; $^{**}P < 0.01$; $^{***}P < 0.001$).

conditions (Fig. 1I). As anticipated, knockdown of GLS1 inhibited protein synthesis in the presence of extracellular glutamine, but these effects were not observed under glutamine starvation conditions (fig. S1R). In addition to supporting protein synthesis, glutamine provides carbon and nitrogen for amino acids, particularly aspartate and asparagine, as well as nucleotide synthesis (*38*). Depletion of GLS1 in the presence of glutamine led to the accumulation of glutamine with decreases in glutamate, aspartate, and asparagine (fig. S1S). In comparison, knockdown of GIRGL increased the intracellular levels of glutamate, aspartate, and asparagine under normal culture conditions and increases in glutamate and aspartate in the absence of glutamine (Fig. 1J). Moreover, under glutamine-replete conditions, GIRGL depletion promoted both RNA and DNA synthesis, though not under glutamine starvation conditions, except for a minor increase in DNA synthesis rates above controls (Fig. 1, K and L, respectively). Predictably, knockdown of GLS1 inhibited RNA and DNA synthesis in the presence of extracellular glutamine, but these effects were entirely diminished under glutamine starvation conditions, which significantly attenuated both processes (fig. S1, T and U). Collectively, these findings indicate that GIRGL inhibits glutamine metabolism through negative regulation of GLS1.

c-Jun positively, whereas HuR negatively, regulates GIRGL expression in response to glutamine deprivation

The gene encoding GIRGL is located on chromosome 7 (20,217,577–20,221,700) and is composed of three annotated transcripts (AC005083.1-201, AC005083.1-202, and AC005083.3), the longest transcript of 740 nucleotides containing all five exons. Notably, GIRGL does not bear significant homology to murine sequences. GIRGL is juxtapositioned in a head-tail orientation with the MACC1 gene, with the next nearest neighboring gene being ITGB8 lying ~110 kb downstream of GIRGL (fig. S2A). Given previous examples where lncRNAs can influence the expression of neighboring genes (*39*), we evaluated whether a co-regulatory relationship existed between MACC1 and GIRGL. Instructively, silencing of MACC1 did not alter GIRGL levels (fig. S2B), and similarly, knockdown of GIRGL failed to influence the expression levels of MACC1 (fig. S2C). Different from GIRGL, glutamine deprivation does not affect MACC1 level (fig. S2D).

We next sought to decipher how glutamine deprivation conditions result in increased levels of GIRGL. We first undertook qPCR assays against intron-specific sequences to assess the production of GIRGL pre-mRNA. Notably, there was a time-dependent increase in all sequences in response to glutamine deprivation (Fig. 2A), thereby confirming that GIRGL is transcriptionally activated under such conditions. To shortlist the likely transcription factors involved, profiling the proximal promoter region of GIRGL in the JASPAR database revealed nine predicted transcription factors involving 16 binding motifs (table S2). Among these candidates, only c-Myc and c-Jun were up-regulated under glutamine deficiency along with a notable increase in the levels of transcriptionally activated c-Jun (Ser^{73}-phosphorylated) (Fig. 2B). Instructively, knockdown of c-Jun, but not c-Myc, reduced the levels of GIRGL in HCT116 cells (Fig. 2C), whereas overexpression of c-Jun led to an increase in GIRGL levels (Fig. 2D). These findings suggested that c-Jun was responsible for the transcriptional up-regulation of GIRGL following glutamine deprivation. Confirming this notion, chromatin immunoprecipitation (ChIP) assays showed that phosphorylated c-Jun bound directly to the GIRGL promoter region [−1238 to −1250 base pairs (bp)] along with a matrix metalloproteinase 1 (MMP1) gene promoter control known to bind with c-Jun (Fig. 2E). Luciferase reporter constructs incorporating this binding site (Fig. 2E) showed that it was responsive to expression of ectopic Flag–c-Jun, and decisively, this activity was abrogated when the binding sequence was mutated (Fig. 2F). However, the levels of GIRGL still increased after silencing of c-Jun in cells subjected to glutamine deprivation (Fig. 3A), suggesting additional regulation beyond transcription level control. The half-life time of GIRGL was prolonged in the presence of transcription inhibitor actinomycin D (Fig. 3B), suggesting that GIRGL was subject to posttranscriptional regulation under these conditions.

Numerous reports indicate that RNA stability can be regulated by HuR (*27*), and we hypothesized that this mechanism may account for the posttranscriptional regulation of GIRGL. Direct interactions between GIRGL and HuR could be observed in RNA pull-down assays against GIRGL and in RNA immunoprecipitation (RIP) assays using antibodies against anti-HuR (Fig. 3, C and D, respectively). Moreover, knockdown of HuR increased GIRGL levels, while its ectopic expression decreased GIRGL levels (Fig. 3, E and F, respectively). Consistently, the half-life of GIRGL was prolonged after silencing of HuR (Fig. 3G). In addition, we considered the impact of glutamine deprivation on the expression of HuR. Examining the levels of HuR revealed a time-dependent decrease in response to glutamine deprivation (Fig. 3H), and as anticipated, the amount of HuR captured in RNA pull-down assays using GIRGL showed less HuR captured under glutamine-deficient conditions (Fig. 3I). Collectively, these results indicate that GIRGL interactions with HuR serve to accelerate its decay.

More recently, it had been reported that HuR functions to destabilize RNAs by facilitating their interactions with let-7/RISC (*28*–*29*). To examine whether HuR regulates GIRGL through a similar mechanism, we determined whether Ago2, a major element of RISC, complexes with HuR and GIRGL. First, reciprocal co-IP analyses using antibodies against HuR and Ago2 verified interactions between endogenous Ago2 and HuR in the HCT116 cell model (fig. S2E). Significantly, GIRGL was recovered in RIP assays against Ago2 (fig. S2F), and as observed with HuR, shRNA-mediated silencing of Ago2 increased the levels of GIRGL (fig. S2G). Moreover, akin to experiments undertaken with HuR, the half-life of GIRGL was prolonged after silencing of Ago2 (fig. S2H). Last, as assessed in RIP assays against either HuR or Ago2, silencing of Ago2 or HuR significantly reduced the relative amount of GIRGL recovered within immunoprecipitates (fig. S2, I and J). Together, our findings indicate that GIRGL turnover is mediated by a HuR/Ago2 (RISC)–mediated mechanism, which appears attenuated under glutamine deprivation conditions.

GIRGL suppresses the translation of GLS1

Having uncovered how GIRGL levels are regulated under glutamine deprivation, we returned to investigate the mechanism(s) by which GIRGL suppresses GLS1 expression. Glutamine depletion caused a time-dependent reduction in GLS1 protein levels in both HCT116 and HT29 cells, while GLS1 expression was maintained at basal levels following knockdown of GIRGL using two independent shRNAs (Fig. 4A and fig. S3A). We considered that GIRGL may physically interact with GLS1, but RNA pull-down assays failed to demonstrate binding between GIRGL and GLS1 protein (Fig. 4B). Moreover, neither glutamine insufficiency nor GIRGL depletion affected the levels of GLS1 mRNA (Fig. 4, C and D, and fig. S3, B

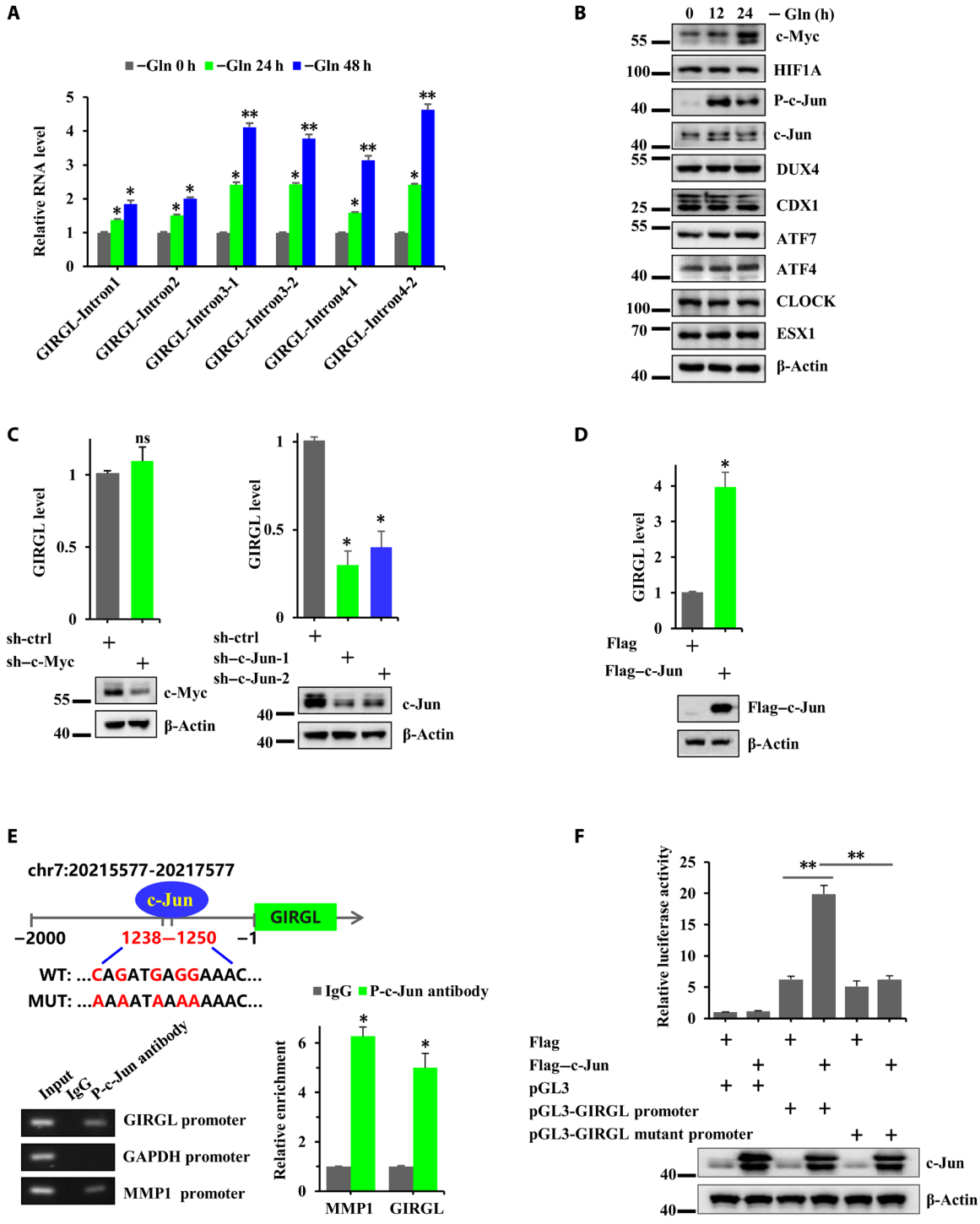

Fig. 2. Glutamine deprivation drives c-Jun–mediated transactivation of GIRGL. (**A**) Exon-specific qPCR measuring GIRGL in HCT116 cells cultured without glutamine for 0 to 48 hours. (**B**) Protein expression of ESX1, CLOCK, ATF4, ATF7, CDX1, DUX1, c-Jun, P-c-Jun, HIF1α, and c-Myc in HCT116 cells in response to glutamine deprivation. β-Actin served as loading control throughout. (**C**) GIRGL (qPCR, top) and c-Myc/c-Jun protein levels (bottom) in HCT116 cells after shRNA-mediated knockdown of c-Myc (left) or c-Jun (right). (**D**) Levels of GIRGL (top) and ectopic c-Jun protein (anti-Flag, bottom) in HCT116 cells transduced with control (pCMV-3×Flag) or Flag–c-Jun (pCMV-3×Flag–c-Jun). (**E**) ChIP assays against control immunoglobulin G (IgG) or anti–p-c-Jun (Ser^{73}) in HCT116 cells targeting the c-Jun consensus binding site within the GIRGL proximal promoter (top). Semiquantitative PCR (bottom left) or qPCR-based detection (bottom right) of GIRGL and negative (GAPDH) and positive (MMP1) controls. (**F**) pGL3-based reporter plasmids were constructed around the c-Jun binding sequence (1238 to 1250) in the GIRGL proximal promoter (E), and dual-luciferase assays were performed in HCT116 cells using pGL3 control or GIRGL reporters containing either wild-type or mutant c-Jun binding sequences (top) with or without ectopic Flag–c-Jun (bottom). (A) and (C) to (F) are mean ± SD; $n = 3$ independent experiments, two-tailed Student's t test. (B) represents three independent experiments (*$P < 0.05$; **$P < 0.01$).

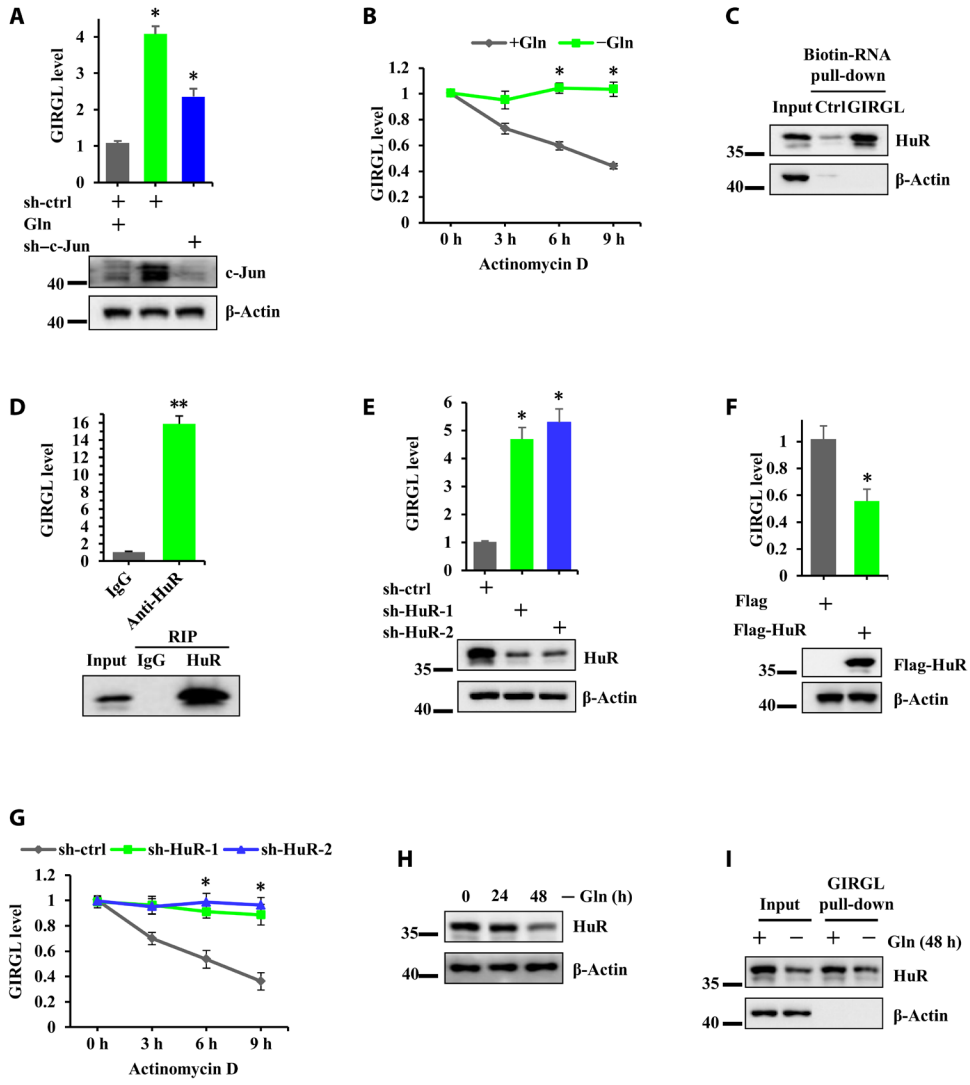

Fig. 3. HuR negatively regulates GIRGL expression under glutamine deprivation. (**A**) GIRGL (qPCR; top) or c-Jun protein levels (bottom) in HCT116 cells after shRNA-mediated knockdown of c-Jun in combination with glutamine depletion. (**B**) Half-life time of GIRGL in HCT116 cells cultured with or without glutamine for 48 hours before addition of actinomycin (5 μg/ml) for 0 to 9 hours. (**C**) RNA pull-down assays were conducted in HCT116 cells against biotin-labeled sense/antisense GIRGL probes, with HuR and β-actin proteins detected by Western blotting. (**D**) RIP assays with IgG or HuR antibodies were performed in HCT116 cells, and the levels of GIRGL (top) and recovered target proteins (bottom) were measured by qPCR and Western blot, respectively. (**E**) GIRGL (qPCR, top) and HuR protein level (bottom) measurements in HCT116 cells after silencing HuR using two independent shRNAs. (**F**) GIRGL levels were determined as per (D) following transduction of control (pCMV-3×Flag) or Flag-HuR (pCMV-3×Flag-HuR) (top). Ectopic HuR was revealed with anti-Flag antibodies (bottom). (**G**) Half-life time of GIRGL in HCT116 cells transduced with shCtrl or shHuR before addition of actinomycin D (5 μg/ml) for 0 to 9 hours. (**H**) HuR protein measurements in HCT116 cells following glutamine deprivation for 0 to 48 hours. (**I**) RNA pull-down assays conducted as per (C) in HCT116 cells cultured with or without glutamine. (A), (B), and (D) to (G) are mean ± SD; $n = 3$ independent experiments, two-tailed Student's t test. (C), (H), and (I) represent three independent experiments (*$P < 0.05$; **$P < 0.01$).

and C), proposing that GIRGL down-regulates GLS1 neither by direct interactions or through transcriptional effects. Analyses using cycloheximide chase assays confirmed that the stability of the GLS1 protein was similar in the presence and absence of GIRGL (Fig. 4E and fig. S3D). Furthermore, the levels of CDH1, the E3 ligase known to target GLS1 for ubiquitin-dependent proteasomal degradation (*40*), were not affected by silencing of GIRGL (Fig. 4F). Notably, inhibition of proteasomal activity with MG132 in cells subjected to glutamine deprivation did not stabilize the levels of GLS1 (Fig. 4G and fig. S3E), thus providing clear evidence that the instability of GLS1 under such conditions is proteasome independent.

On the basis of the latter findings, we hypothesized that GIRGL regulates GLS1 levels via translational control. Consequently, we estimated protein translation levels using polysome profiling assays. Compared with normal culture conditions, the absence of glutamine per se did alter the assembly of polysomes associated with GLS1 mRNA. However, the formation of elongating polysomes containing GLS1 was decreased (Fig. 4H), indicating a reduction in the levels of translated GLS1 mRNA in the absence of glutamine. Manipulation of GIRGL by either knockdown or overexpression resulted, respectively, in either decreased or increased formation of ribosomal and polyribosome assembly involving GLS1 mRNA

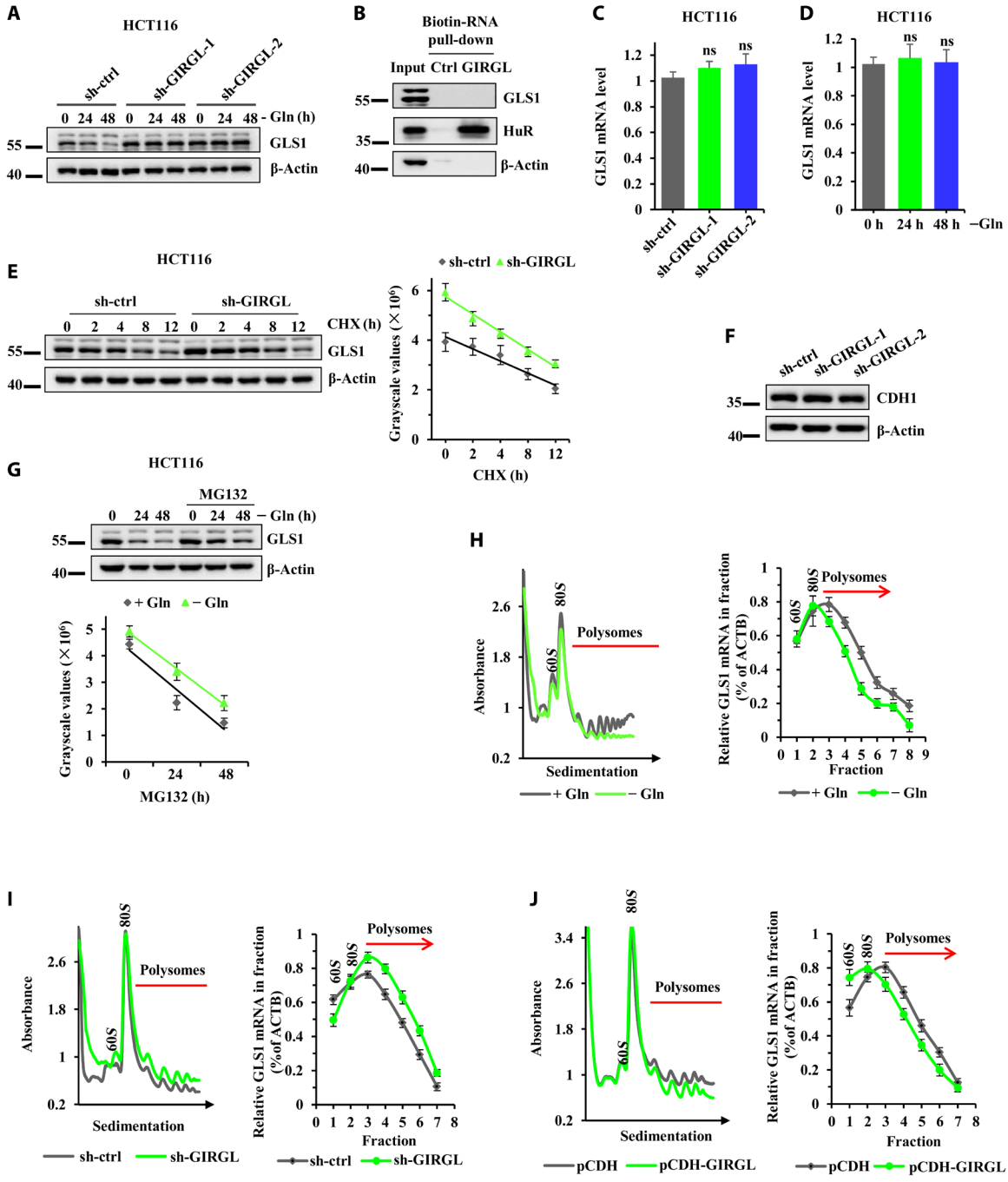

Fig. 4. GIRGL suppresses the translation of GLS1. (**A**) GLS1 protein levels in HCT116 cells transduced with shCtrl or independent shRNAs against GIRGL (shGIRGL-1, shGIRGL-2) after culture without glutamine (0 to 48 hours). β-Actin served as loading control. (**B**) GLS1, HuR, or β-actin proteins captured in RNA pull-down assays using HCT116 cell lysates against biotin-labeled sense (Ctrl) or antisense GIRGL probes. (**C** and **D**) GLS1 mRNA levels in HCT116 cells after transduction with shCtrl or independent shRNAs against GIRGL (C) or cultured without glutamine for 0 to 48 hours (D). (**E**) GLS1 protein levels in HCT116 cells transduced with shCtrl or shGIRGL after treatment with 50 μM cycloheximide (CHX) for 0 to 12 hours (left). Densitometric analyses (right). (**F**) CDH1 protein expression after silencing of GIRGL in HCT116 cells using two independent shRNAs. (**G**) GLS1 protein levels in HCT116 cells treated with or without 20 μM MG132 for 6 hours following culture without glutamine for 0 to 48 hours (top). Densitometric analyses (bottom). (**H**) Velocity sedimentation analysis of HCT116 cells treated with or without glutamine for 48 hours. Continuous OD_{254nm} measurements show resolution of 60*S* ribosomes, 80*S* monosome complex, and polysomes (left). The abundance of GLS1 mRNA relative to actin (right). (**I**) Velocity sedimentation as per (H) in HCT116 cells transduced with either shCtrl or shGIRGL-1. (**J**) Velocity sedimentation as per (H) in HCT116 cells transduced with either PCDH or PCDH-GIRGL. (A), (B), and (E) to (G) represent three independent experiments. (C), (D), and (H) to (J) are mean ± SD; $n = 3$ independent experiments, two-tailed Student's *t* test.

(Fig. 4, I and J). Together, these results establish that the downregulation of GLS1 observed after glutamine deprivation results from the GIRGL-mediated translational suppression of GLS1 mRNA.

LncRNA GIRGL cooperates with CAPRIN1 to suppress translation of *GLS1*

To investigate the mechanism responsible for GIRGL-mediated suppression of GLS1, we interrogated the protein interactome of GIRGL using RNA pull-down assays. Mass spectrometry (MS) was used to identify proteins that specifically coprecipitated with biotin-labeled antisense GIRGL but not the control (Fig. 5, A and B). Top four candidate proteins were further verified by Western blotting (Fig. 5C), and only GRP78 was found to be unable to interact with GIRGL. Consistently, RIP assays confirmed that GIRGL was robustly retrieved within anti-CAPRIN1 or anti-G3BP1 immunoprecipitates (Fig. 5D). Because G3BP1 exists as a homodimer or heterodimer with G3BP2 (*41*), we also established that G3BP2 coprecipitates with GIRGL (Fig. 5C). Of note, the most prevalent candidate identified by MS was HNRPM, but because it is frequently recovered in RNA binding protein screens, presumably because of its role in pre-mRNA binding (*42*–*43*), we did not consider it further. G3BPs are known to bind CAPRIN1 to promote SG formation (*36*). We therefore examined whether the individual SG components were co-regulated or whether their levels affected GLS1 expression. However, individual knockdown assays against G3BP1, G3BP2, or CAPRIN1 revealed no resulting changes in the respective SG components (fig. S4, A to C). Knockdown of HNRPM also failed to affect GLS1 levels (fig. S4D). Notably, only knockdown of CAPRIN1 caused increased GLS1 levels in contrast to experiments with G3BP1 and G3BP2, which failed to influence GLS1 expression. Moreover, GLS1 level will not be reduced upon glutamine deficiency if CAPRIN1 is depleted (fig. S4E), indicating that glutamine insufficiency–induced GLS1 reduction is required for CAPRIN1. Consistently, the forced expression of CAPRIN1 reduced GLS1 expression (Fig. 5E). Notably, GIRGL overexpression was unable to suppress GLS1 expression following the depletion of CAPRIN1 (Fig. 5F), suggesting that CAPRIN1 is functionally required for GIRGL-mediated inhibition of GLS1 translation. Polyribosome profiling analysis performed in CAPRIN1-depleted cells phenocopied the effects seen following GIRGL silencing, with notable increases in the formation of polyribosome and associated translatable GLS1 mRNA (Fig. 5G). Thus, these data collectively indicate that CAPRIN1 cooperates with GIRGL to suppress the translation of GLS1 mRNA.

Previous reports have highlighted the role of cytosolic CAPRIN1 in mRNA transport and translation, with selective binding reported for c-Myc and cyclin D2 mRNAs occurring through a highly conserved arginine-glycine-glycine repeat (RGG) domain present in its C-terminal region (*31*). These observations proposed that CAPRIN1 may also physically interact with GLS1 mRNA. Upholding this notion, RNA pull-down assays demonstrated that CAPRIN1 was selectively captured with GLS1 mRNA (Fig. 6A), while GLS1 mRNA was markedly enriched in RIP assays against CAPRIN1 (Fig. 6B). Moreover, we observed that GLS1 mRNA and GIRGL were also reciprocally captured in RNA pull-down assays against GIRGL and GLS1, respectively (Fig. 6C). Instructively, silencing of CAPRIN1 reduced the association between GLS1 mRNA and GIRGL (Fig. 6D), indicating that CAPRIN1 forms a ternary complex with GIRGL and GLS1 mRNA. However, knockdown of GIRGL also diminished the association between CAPRIN1 and GLS1 mRNA (Fig. 6E), suggesting that GIRGL regulates the association between CAPRIN1 and GLS1 mRNA and is thus a necessary element in suppression of GLS1 translation. As expected from this interpretation, RNA pull-down analyses undertaken against GIRGL in cells subjected to glutamine deprivation demonstrated enhanced recovery of CAPRIN1 and GLS1 mRNA compared to cells cultured under glutamine-replete conditions (Fig. 6F).

GIRGL promotes homodimerization of CAPRIN1 and forms a quaternary complex with GLS1 mRNA

We extended our investigations to understand how GIRGL binding to CAPRIN1 influences its function. First, silencing of GIRGL showed no effect on the expression levels of CAPRIN1 (Fig. 7A). It has been reported that CAPRIN1 functions as homodimer whose formation is mediated via amino acid residues 132 to 251 (*44*) present within the conserved HR1 region (fig. S5A). Notably, after chemical cross-linker treatment using disuccinimidyl suberate (DSS), dimers rather than monomers were the predominant form of endogenous CAPRIN1 captured in pull-down assays against GLS1 mRNA (fig. S5B), consistent with the notion that CAPRIN1 is present in dimeric form when it inhibits GLS1 translation. On the basis of the requirement for GIRGL binding in CAPRIN1 function established above, we postulated that GIRGL might affect the dimerization of CAPRIN1. shRNA silencing of GIRGL decreased, whereas GIRGL overexpression increased, the amount of CAPRIN1 dimers detected in HCT116 cell total protein extracts captured through chemical cross-linking (Fig. 7, B and C). Furthermore, as seen in experiments using GLS1 mRNA (fig. S5B), more CAPRIN1 dimers than monomers were retrieved in pull-down assays against GIRGL (Fig. 7D). Together, these results imply that GIRGL promotes CAPRIN1 dimerization, which captures GLS1 mRNA and inhibits its translation.

To better define the complex between dimerized CAPRIN1, GIRGL, and GLS1 mRNA, we used epitope-tagged CAPRIN1 constructs. We then undertook two-step IPs from cells expressing Flag and hemagglutinin (HA)–tagged CAPRIN1. In the first-phase IP using anti-Flag antibodies, HA-CAPRIN1 and GIRGL were recovered with Flag-CAPRIN1, whereas conversely after elution and secondary IP against HA, both Flag-CAPRIN1 and GIRGL were coprecipitated (Fig. 7E), further indicating that GIRGL forms a ternary structure with dimerized CAPRIN1.

Last, experiments were undertaken to map the interacting regions responsible for binding between CAPRIN1, GIRGL, and GLS1 mRNA. In addition to full-length Flag-tagged CAPRIN1, a series of truncates (amino acids 1 to 322, 323 to 606, and 323 to 709) were constructed (fig. S5A) and used in RIP assays using anti-Flag antibodies. As anticipated, both GIRGL and GLS1 mRNA were robustly recovered with full-length CAPRIN1 (fig. S5, C and D, respectively). Among the truncated forms of CAPRIN1, GIRGL only bound to amino acids 1 to 322, whereas GLS1 mRNA showed strong affinity for amino acids 323 to 709, indicating that the HR1 and E-rich domains (amino acids 1 to 322) of CAPRIN1 are responsible for interactions with GIRGL, while the RGG motif (amino acids 607 to 709) is responsible for its binding to GLS1 mRNA.

Conversely, to determine which regions within GIRGL and GLS1 mRNA are responsible for their interactions with CAPRIN1, in vitro transcribed RNAs were used in pull-down assays to detect CAPRIN1 binding. On the basis of the asymmetrical form predicted

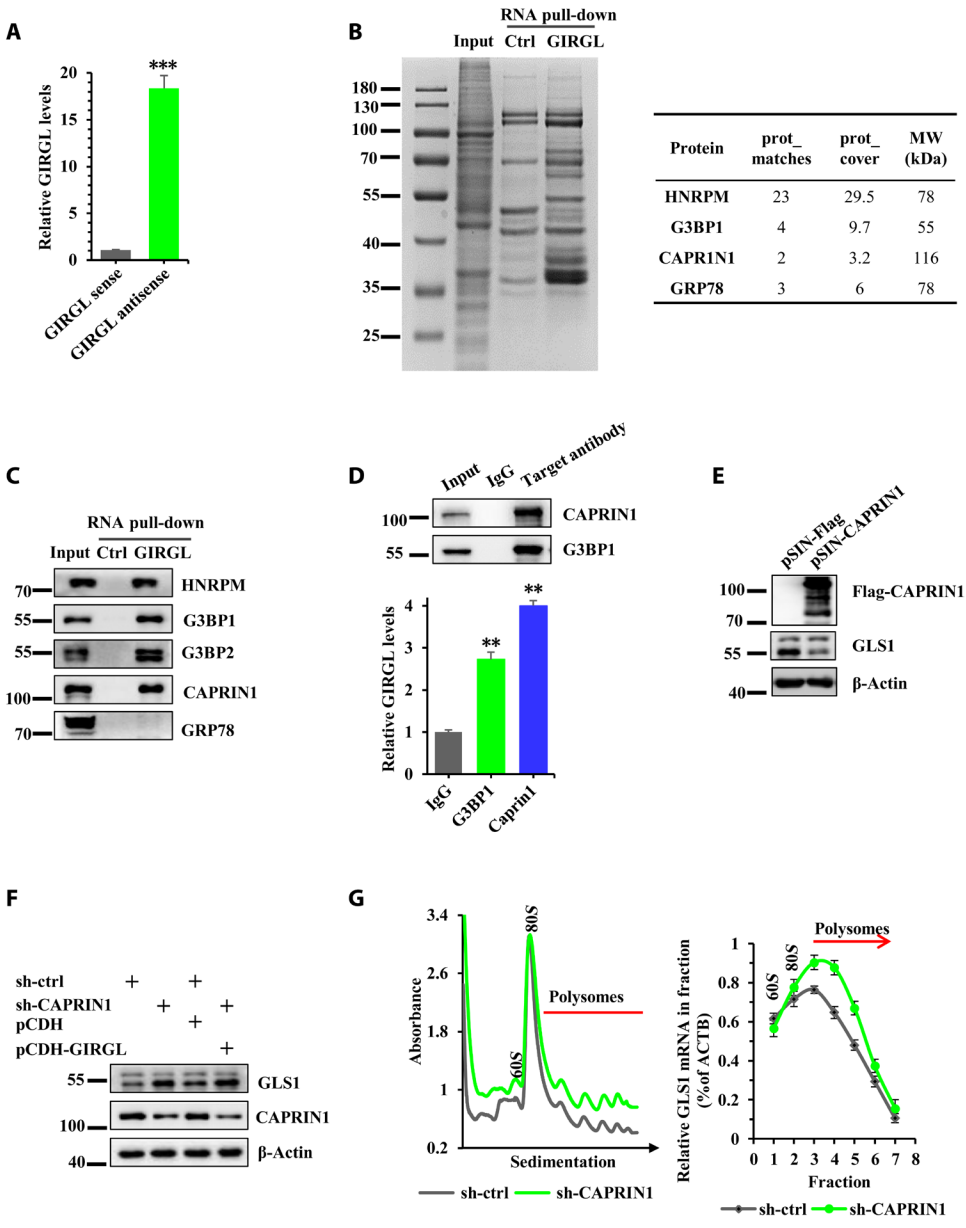

Protein	prot_ matches	prot_ cover	MW (kDa)
HNRPM	23	29.5	78
G3BP1	4	9.7	55
CAPR1N1	2	3.2	116
GRP78	3	6	78

Fig. 5. GIRGL cooperates with CAPRIN1 to suppress GLS1 translation. (**A** and **B**) GIRGL levels recovered using biotin-labeled sense/antisense GIRGL probes in RNA pull-down assays against HCT116 cells (A). SDS–polyacrylamide gel electrophoresis (left) and MS identified protein IDs (right) (B). (**C**) Putative GIRGL-binding proteins from (B) evaluated using Western blotting. (**D**) RIP assays performed against HCT116 cells using IgG, G3BP1, or CAPRIN1 antibodies. Western blot (top) with GIRGL levels (bottom). (**E**) GLS1 protein levels in HCT116 cells following transduction of control (Psin-3×Flag) or CAPRIN1 (Psin-3×Flag-CAPRIN1) vectors. Ectopic CAPRIN1 revealed using anti-Flag. (**F**) GLS1 protein levels in HCT116 cells following transduction of shCtrl, shCAPRIN1, shCtrl plus PCDH, and shCAPRIN1 plus PCDH-GIRGL. (**G**) Velocity sedimentation analysis of HCT116 cells transduced with shCtrl or shCAPRIN1. Polysome profiles (left) and abundance of GLS1 mRNA (right). (A), (D), and (G) are mean ± SD; $n = 3$ independent experiments, two-tailed Student's t test. (C), (E), and (F) represent three independent experiments (**$P < 0.01$; ***$P < 0.001$).

by its secondary structure, we divided GIRGL into two fragments for this analysis (nucleotides 1 to 424 and nucleotides 424 to 740; fig. S5E). RNA pull-down assays showed that Flag-CAPRIN1 was selectively recovered with sense, but not antisense, GIRGL, while only fragment2 (nucleotides 424 to 740), but not fragment1 (nucleotides 1 to 424), supported CAPRIN1 binding (fig. S5F). We further dissected the predicted symmetrical Y-shaped configuration of fragment2 by individually deleting each arm from the GIRGL sequence. However, neither the GIRGL-arm1 nor the GIRGL-arm2 deletion mutants promoted the dimerization of CAPRIN1 (fig. S5G), proposing that the predicted symmetrical Y-shaped configuration is responsible for dimer binding. Moreover, dividing the GLS1 mRNA into 5′ untranslated region (5′UTR), coding sequence, and two 3′UTR sequences (3′UTR-1 and 3′UTR-2) and repeating the pull-down assays revealed binding between Flag-CAPRIN1 and 3′UTR-1 of GLS1 mRNA (fig. S5H). Thus, GIRGL associates with CAPRIN1 within its HR1-E–rich domain, whereas its interaction with the 3′UTR of GLS1 mRNA occurs distinctly via its RGG motif.

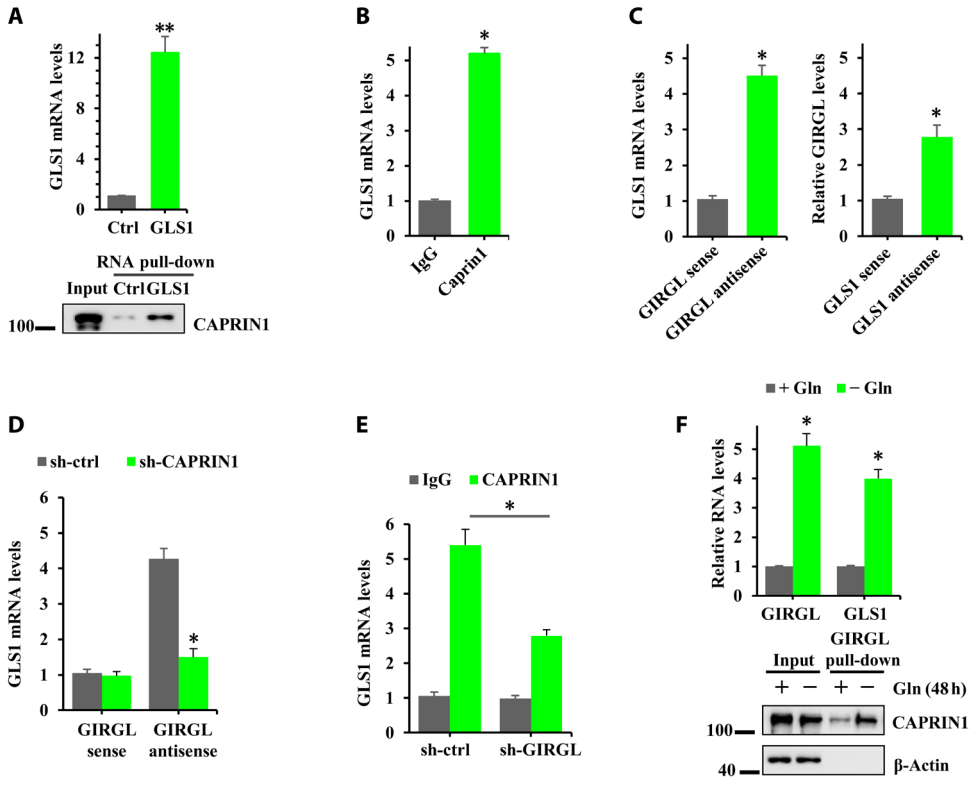

Fig. 6. GIRGL promotes association between CAPRIN1 and GLS1 mRNA. (**A**) GLS1 mRNA (top) and CAPRIN1 protein levels (bottom) recovered with biotin-labeled sense (Ctrl) or antisense GLS1 probes in RNA pull-down assays against HCT116 cells. (**B**) GLS1 mRNA levels measured by qPCR in IgG and CAPRIN1 antibody RIP assays performed against HCT116 cell lysates. (**C**) Reciprocal RNA pull-down assays performed with sense/antisense GIRGL probes (left) or GLS1 probes (right) against HCT116 cells with recovery of GLS1 mRNA or GIRGL measured by qPCR. (**D**) GLS1 mRNA levels in RNA pull-down assays against GIRGL performed as per (C) after transducing cells with shCtrl or shCAPRIN1. (**E**) GLS1 mRNA levels in RIP assays conducted as per (B) in cells transduced with either shCtrl or shGIRGL. (**F**) GIRGL and GLS1 mRNA (top) and CAPRIN1 protein levels (bottom) recovered using antisense GIRGL probes in RNA pull-down assays using cells cultured with or without glutamine for 48 hours. (A) to (F) are mean ± SD; $n = 3$ independent experiments, two-tailed Student's t test (*$P < 0.05$; **$P < 0.01$).

GIRGL promotes phase separation of CAPRIN1-GLS1 mRNA complexes into SGs

After establishing the nature of the GIRGL-CAPRIN1-GLS1 mRNA complex, we returned to consider how this physiologically integrates within the context of glutamine deprivation. Because CAPRIN1 has been associated with both SG formation and translational control (*34*, *36*), we considered that GIRGL may exert its actions in the context of SGs. Overexpression of SG proteins can initiate SG formation in the absence of stress (*31*), and we confirmed that this phenomenon occurs with CAPRIN1 in our experimental system. Enforced expression of enhanced GFP (EGFP)–CAPRIN1 generated fluorescent punctate structures, which did not overlap with the lipid membrane marker DiI (fig. S5I). Instructively, ectopic expression of GIRGL resulted in the coalescence of endogenous CAPRIN1 into similar punctate structures (Fig. 7F), suggesting that GIRGL mediates SG formation. There was costaining observed between CAPRIN1 and the SG markers G3BP1 and TIA1 (Fig. 7F and fig. S5J, respectively), identifying these structures as SGs. Extending this analysis to a fully endogenous context, multicolor confocal analysis of GLS1 mRNA, GIRGL, and CAPRIN1 showed that their largely diffuse cytoplasmic staining under glutamine-replete conditions shifted to highly colocalized punctate structures in the absence of glutamine (Fig. 7G). Consistently, the latter structures demonstrated costaining between CAPRIN1 and G3BP1 or TIA1 (fig. S5, K and L, respectively). Together, these data indicate that GIRGL promotes CAPRIN1-dependent SG formation under glutamine deprivation conditions and that the resulting SGs capture GLS1 mRNA.

SGs form through liquid-liquid phase separation, resulting from the aggregation of SG component proteins that interact through intrinsically disordered (ID) regions (*45*). This process can be modeled in vitro and, for example, has been used to show how posttranslational modifications of the fragile X mental retardation protein (FMRP) affect its phase separation with RNA (*46*). Using this approach, we observed the formation of visible droplets (phase-separated protein-rich condensates) when Flag-CAPRIN1 was incubated with 3′UTR-1 of GLS1, but not with the GLS1 5′UTR (Fig. 7H and fig. S5M). Formation of the CAPRIN1-containing condensates was dependent on the concentration of 3′UTR-1 GLS1 mRNA (fig. S5N), and moreover, these droplets were observed to undergo fusion events (fig. S5O), characteristic of protein droplets formed by liquid-liquid phase separation. Notably, the frequency of phase droplet formation between CAPRIN1 and GLS1 mRNA was comparatively increased when full-length sense, but not antisense, GIRGL was added to these assays (Fig. 7I and fig. S5P), suggesting that GIRGL increases the rate of phase droplet formation between CAPRIN1 and GLS1 mRNA. We additionally used FRAP (fluorescence recovery after photobleaching) to study the mobility of CAPRIN1 and GLS1–3′UTR-1 within droplets. Monitoring fluorescence signals in the photobleached

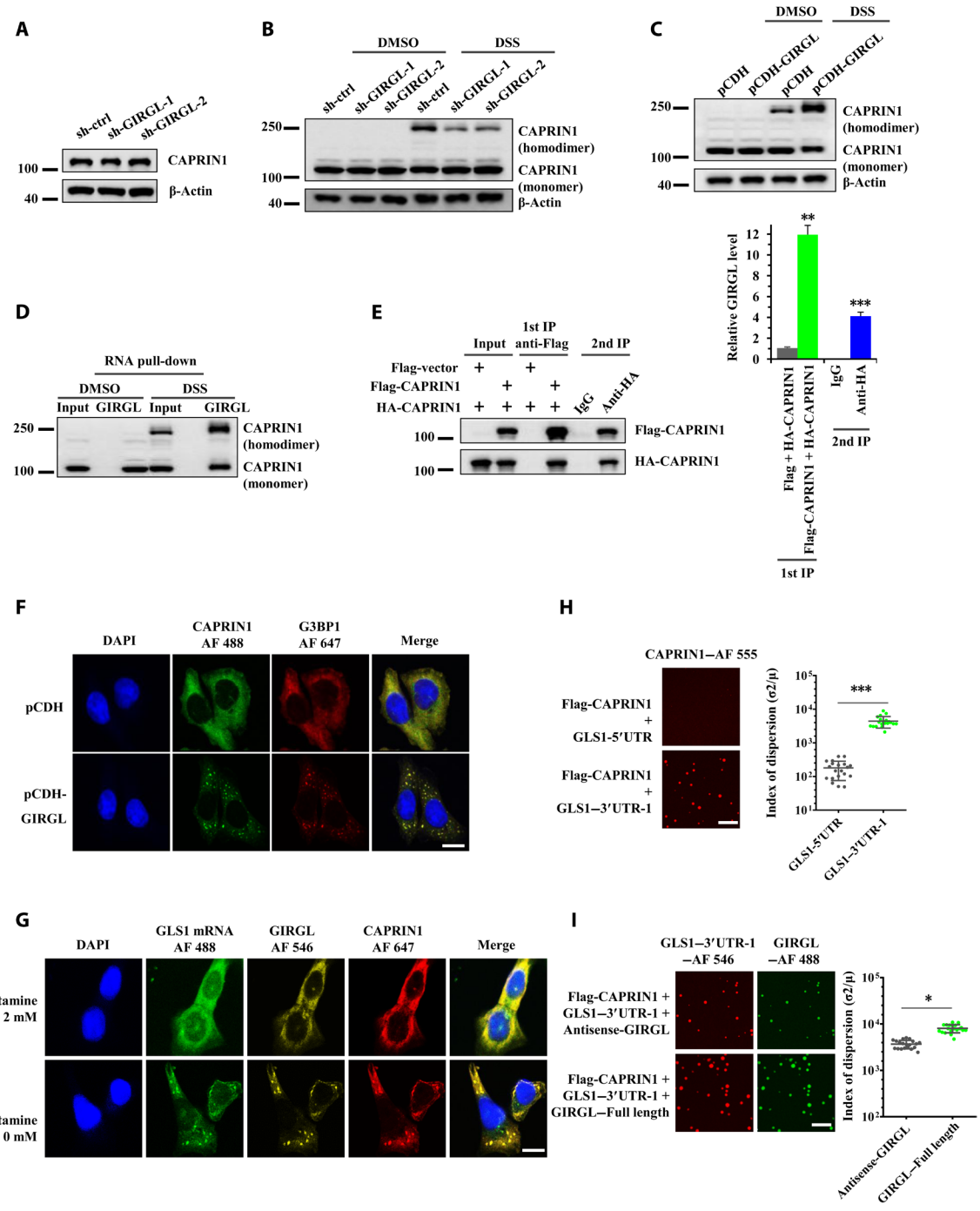

Fig. 7. GIRGL promotes CAPRIN1 dimerization, phase separation, and SG formation. (**A**) CAPRIN1 protein expression in HCT116 cells transduced with shCtrl or two independent shRNAs targeting GIRGL. β-Actin loading control was used throughout. (**B**) HCT116 cells as per (A) were treated with disuccinimidyl suberate (DSS) or dimethyl sulfoxide (DMSO) before analysis of CAPRIN1 homodimerization. (**C**) CAPRIN1 homodimerization as per (B) in HCT116 cells transduced with PCDH or PCDH-GIRGL. (**D**) CAPRIN1 homodimerization in GIRGL RNA pull-down samples from DMSO- or DSS-treated HCT116 cells. (**E**) Western blotting against Flag-CAPRIN1, HA-CAPRIN1 (left), and GIRGL qPCR (right) in two-step IPs conducted in HCT116 cells transfected with Flag-vector/HA-CAPRIN1 or Flag-CAPRIN1/HA-CAPRIN1. (**F**) Confocal images showing CAPRIN1 (green), G3BP1 (red), and DAPI (blue) staining in HCT116 cells transduced with PCDH or PCDH-GIRGL (scale bar, 10 μm). (**G**) Confocal images of GLS1 mRNA (FISH, green), GIRGL (FISH, yellow), and CAPRIN1 (IF, red) in HCT116 cells cultured with or without 2 mM glutamine for 48 hours (scale bar, 10 μm). (**H**) Recombinant Alexa Fluor 555–labeled Flag-CAPRIN1 (20 μM) was incubated with either GLS1 mRNA 3′UTR-1 or 5′UTR (0.2 μM) at room temperature. Epifluorescence images were collected to observe liquid-liquid phase separation droplets (left) (scale bar, 30 μm), and the normalized variance of droplets was measured as the index of dispersion (σ2/μ) (right). (**I**) Epifluorescence images were collected as per (H) after incubating Flag-CAPRIN1 (20 μM) with Alexa Fluor 546–labeled GLS1 mRNA 3′UTR-1 (0.2 μM) and Alexa Fluor 488–labeled sense-GIRGL or antisense-GIRGL (0.2 μM) at room temperature (left) (scale bar, 30 μm), and the normalized variance of droplets was measured as the index of dispersion (σ2/μ) (right). (A) to (D), (F), and (G) represent three independent experiments. (E), (H), and (I) are mean ± SD; $n = 3$ independent experiments, two-tailed Student's t test (*$P < 0.05$; **$P < 0.01$; ***$P < 0.001$).

window indicated that there was a time-dependent recovery in CAPRIN1 (72 ± 8% mobile fraction values, $T_{1/2}$ = 32 ± 3 s, mean ± SD) and GLS1–3′UTR-1 (70 ± 6% mobile fraction values, $T_{1/2}$ = 33 ± 4 s) signals with similar recovery kinetics (fig. S5Q). Comparable analyses of FRAP signals for GLS1–3′UTR-1 (67 ± 5% mobile fraction values, $T_{1/2}$ = 23 ± 2 s) versus GIRGL (62 ± 9% mobile fraction values, $T_{1/2}$ = 25 ± 4 s) in CAPRIN1-formed droplets again showed similar recovery characteristics (fig. S5R), together indicating that CAPRIN1, GLS1–3′UTR-1, and GIRGL are intrinsically fluid and part of the same mobile fraction within the droplets. Thus, the findings of the biophysical experiments fully support the notion that GIRGL contributes to CAPRIN1-dependent SG formation in association with GLS1 mRNA.

Biological implications of GIRGL in tumorigenesis

We next considered the fundamental impact of GIRGL on cancer cell growth under normal and glutamine-depleted conditions. Under normal 2 mM levels of glutamine supplementation, silencing of GIRGL increased, whereas its overexpression inhibited the growth of HCT116 cell proliferation (Fig. 8A). The growth-enhancing effect of GIRGL silencing was further pronounced after lowering the glutamine levels to 0.4 mM (Fig. 8B), but notably, in the complete absence of glutamine, the number of cells markedly decreased after 2 days when GIRGL was depleted (Fig. 8C, top). Furthermore, ectopic expression of GIRGL potentiated cell growth when glutamine is absent, proposing that GIRGL plays a survival function during glutamine deficiency stress (Fig. 8C, bottom). Similarly, the growth-inhibitory effects of GIRGL were recapitulated in colony formation assays using HCT116 cells (Fig. 8, D and E).

Supplementary experiments were then used to verify the functional relationship between GIRGL and GLS1. First, under glutamine-replete conditions, GIRGL knockdown promoted cell growth, which could be reversed by GLS1 knockdown (fig. S6A). Consistently, the ectopic expression of GLS1 substantially reversed the growth-inhibitory phenotype resulting from GIRGL overexpression (fig. S6B). Second, depletion of GLS1 in combination with GIRGL shRNA during glutamine starvation prevented the loss of cell viability observed after GIRGL depletion and long-term culture (fig. S6C). Moreover, while GIRGL overexpression restored modest steady-state growth in the absence of glutamine, ectopic GLS1 expression erased the ability of GIRGL to preserve cell viability and growth (fig. S6D). Last, to cement the functional relationship between GIRGL and GLS1, we examined the combined effects of GLS1 knockdown and GIRGL overexpression under glutamine-deprived conditions. Informatively, overexpression of GIRGL in GLS1-knockdown cells showed little impact on the cell viability or growth (fig. S6E). This, together with the preceding experiments, indicates that GIRGL actions substantially involve GLS1. In addition, by extension, this suggests that GLS2 is unlikely to be involved in the GIRGL-dependent regulation of cell survival under glutamine-deprived conditions.

Last, we considered the impact of GIRGL on tumorigenicity and examined the growth of HCT116 cells as xenografted tumors in nu/nu mice. Consistently, depletion of GIRGL markedly increased growth in vivo, while its enhanced expression decreased tumor growth (Fig. 8, F and G). We further conducted an assessment of GIRGL expression in a cohort of 30 pairs of colon cancer versus normal tissues. This analysis showed that approximately half of cases exhibited markedly higher GIRGL levels in tumors compared to their normal adjacent tissues, while others were unchanged or slightly reduced (Fig. 8H). Our working model linking GIRGL, GLS1 and the impact of glutamine deprivation is shown in Fig. 9.

DISCUSSION

The limiting vasculature of the tumor microenvironment combined with competition among cancer cells can result in localized nutrient deficiencies (*47*–*48*). Consequently, cancer cells must strategically counter the fluctuating levels of even abundant nutrients such as glutamine. Previous studies have revealed plasticity in cancer cell metabolism during adaptation to glutamine deprivation (*49*–*50*). For example, HCT116 colon cancer cells maintain energy production and cell viability by promoting de novo synthesis of glutamine and glutamate (*49*). Nevertheless, prolonged glutamine starvation compromises cell viability (*51*), and therefore, a balance must be struck between promoting proliferation and ensuring cell survival. Here, we considered the effects of glutamine fluctuations on glutaminase, the key initiating enzyme involved in glutaminolysis. Consistent with the emerging theme that the glutaminase isoform GLS1 is most relevant to tumorigenesis (*11*, *13*), we observed that depriving colon cancer cells of glutamine decreased the levels of GLS1, while the levels of GLS2 remained unaffected. The levels of GLS1 diminish gradually and proportionally to the availability of glutamine, indicating that rapid changes in glutaminase function are neither warranted nor advantageous.

Glutamine deprivation is known to induce the proto-oncogene c-Myc (*18*), which has been reported to up-regulate GLS1 through its repression of posttranscriptional mechanisms mediated by miR-23a/b (*12*) and the lncRNA GLS-AS (*24*). Consistently, we found that glutamine deprivation stress also increased c-Myc expression, but we did not observe up-regulation of GLS1. Rather, our efforts to understand the mechanisms controlling GLS1 expression revealed the involvement of GIRGL, an lncRNA that negatively regulates GLS1 through a mechanism that appears independent of c-Myc. GIRGL was shown to restrain mitochondrial respiration, suggesting that it contributed to the efficacious utilization of available glutamine, thus ensuring that limiting substrate amounts will not be exhausted. Subsequent investigations addressed two main aspects of the relationship between the levels of glutamine, GIRGL, and GLS1: the first being the basis for the up-regulation of GIRGL under limiting glutamine conditions and, second, how the increased expression of GIRGL affects the expression of GLS1.

We observed that GIRGL was up-regulated in a time- and concentration-dependent manner in cancer cells in response to glutamine deficiency. Previous studies have shown that glutamine deficiency invokes stress-activated Jnk/c-Jun signaling (*52*–*53*), and consistently, we found that glutamine deficiency resulted in the activation of c-JUN. GIRGL was transcriptionally driven by c-JUN, although the levels of GIRGL were not maintained by c-JUN alone. GIRGL levels were destabilized through recruitment to RISC, a process mediated by its binding to the RNA binding protein HuR. Although HuR is known for its role as a stabilizer of mRNAs or lncRNAs (*27*), more recent investigations have shown that HuR also promotes RNA degradation as observed with c-Myc mRNA and lincRNA-p21 (*28*–*29*). Thus, the basal levels of GIRGL appear to be maintained through comparatively low transcription combined with its turnover by RNA silencing. Following glutamine deprivation, GIRGL levels are up-regulated by the combination of c-Jun–mediated transcriptional increases along with a significantly

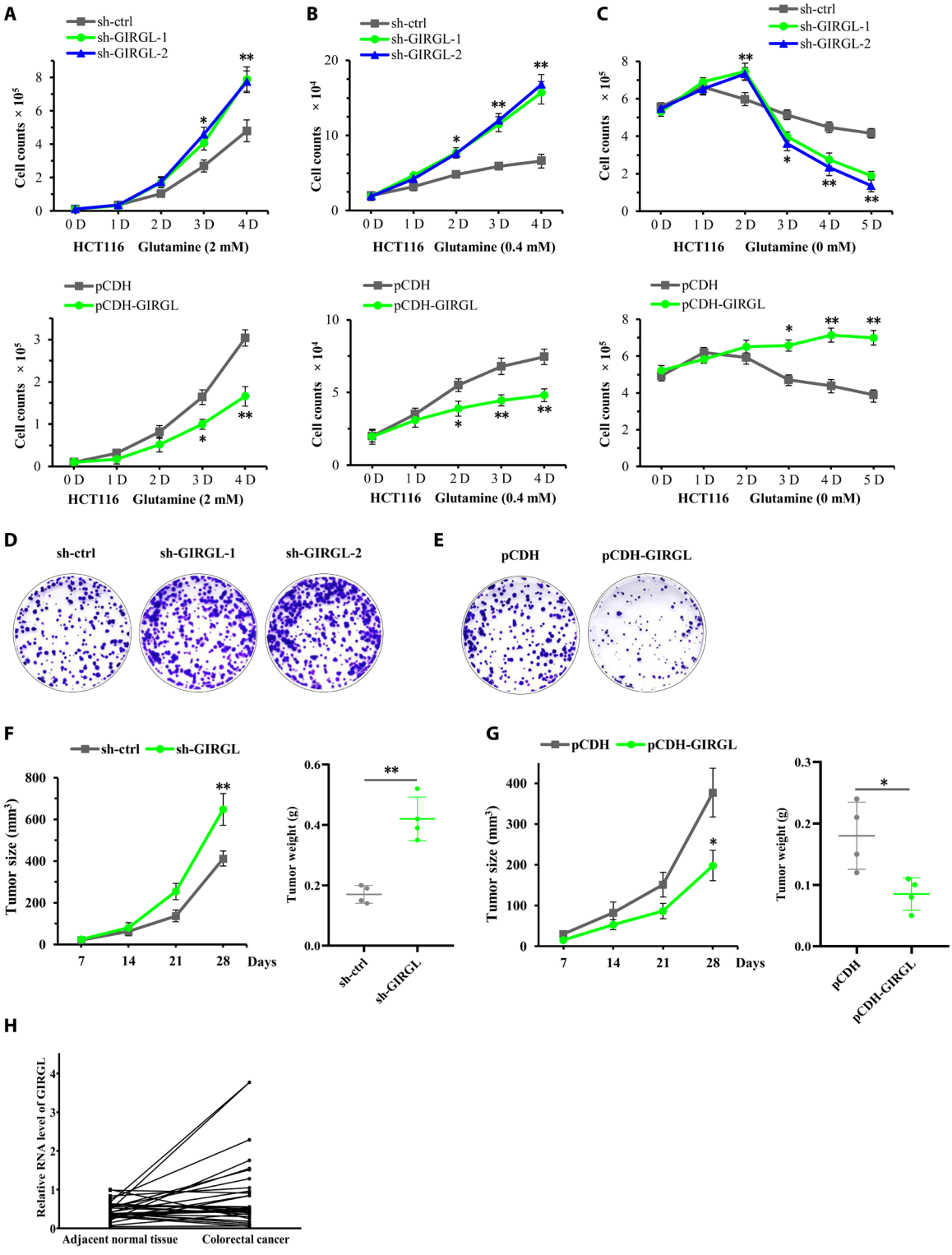

Fig. 8. Biological implications of GIRGL in tumorigenesis. (**A** to **C**) HCT116 cells were transduced with shCtrl or with one of two independent shRNAs targeting GIRGL (upper) and PCDH or PCDH-GIRGL (bottom) before culturing in 2 mM (A), 0.4 mM (B), and 0 mM (C) glutamine. Cell numbers were counted over consecutive days to assess proliferation. (**D** and **E**) Silencing of GIRGL promotes, whereas overexpression of GIRGL inhibits, the clonogenic potential of HCT116 cells. (**F** and **G**) HCT116 cells (2×10^6) transduced with shCtrl or shGIRGL-1 (F) or PCDH or PCDH-GIRGL (G) were inoculated into opposite flanks of nu/nu mice. Tumor sizes were measured at the indicated time points (left) and excised and weighed after 4 weeks (right) after mice were humanely culled. (**H**) Relative GIRGL expression among 30 pairs of matched colorectal cancer and adjacent normal tissues determined by qPCR. (A) to (C), (F), and (G) are mean ± SD; $n = 3$ independent experiments, two-tailed Student's t test. (D) and (E) represent three independent experiments (*$P < 0.05$; **$P < 0.01$).

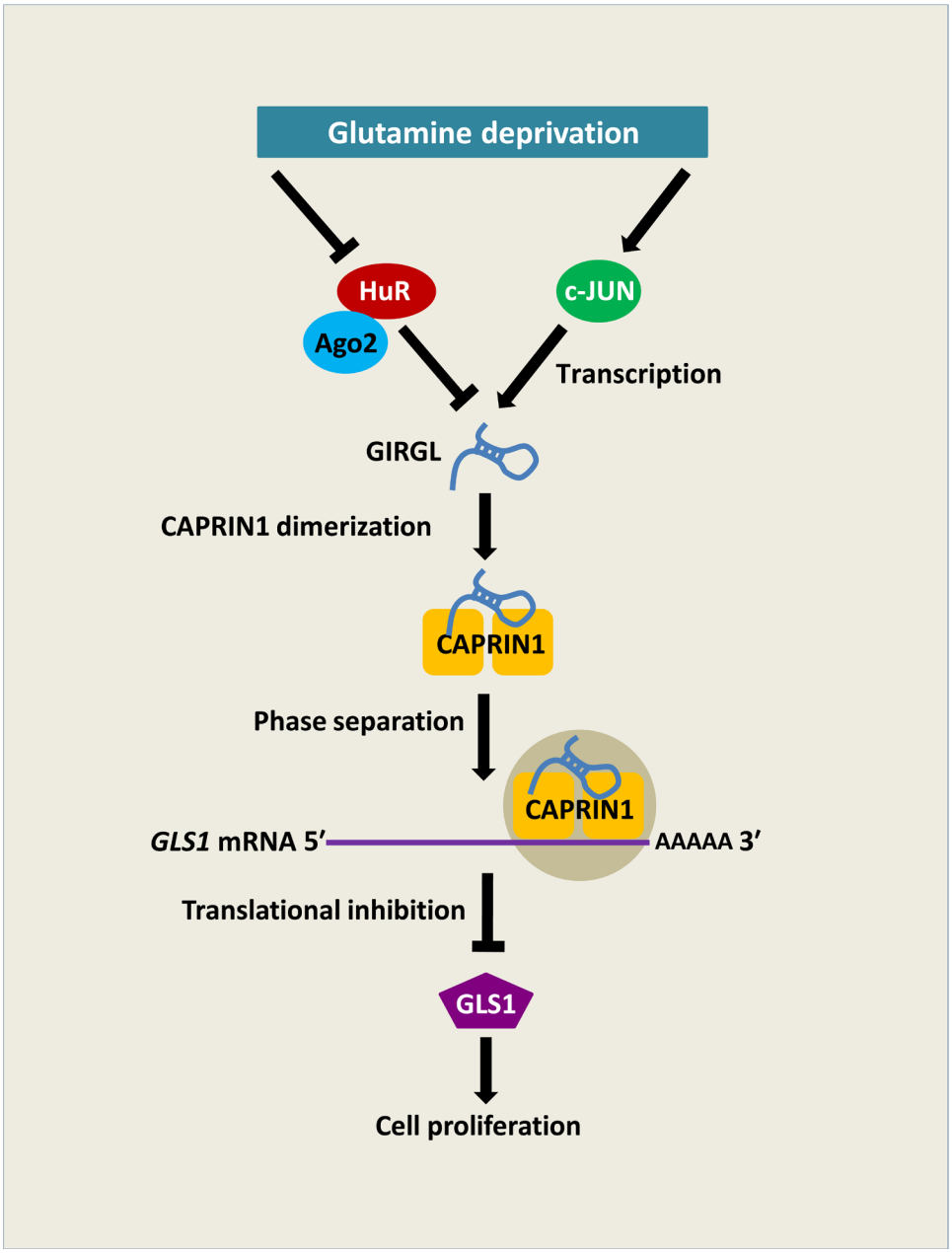

Fig. 9. Working model for induction of GIRGL expression and down-regulation of GLS1 under glutamine deprivation conditions.

longer half-life, where, consistently, HuR levels are down-regulated. These dual mechanisms therefore constitute a feedback loop responsible for maintaining GIRGL levels in response to glutamine availability.

With respect to the inhibitory effects of GIRGL on GLS1 levels, we showed that the underlying basis involved decreased GLS1 translation. The mechanism involved formation of complex between GIRGL, GLS1 mRNA, and the RNA binding proteins, CAPRIN1 and G3BP. It has been previously established that CAPRIN1, G3BP1, and G3BP2 collude to promote the translation of PKR (double-stranded RNA-dependent protein kinase) and IFITM2 (interferon-induced transmembrane protein 2) mRNAs during the antiviral response against dengue virus (*35*). Moreover, dengue-derived subgenomic ncRNAs were shown to inhibit the translation of PKR and IFITM2 mRNAs by binding to CAPRIN1, G3BP1, and G3BP2 (*35*). An additional report in murine macrophage showed that CAPRIN1 also stabilized signal transducer and activator of transcription 1 (Stat1) mRNA, but its levels were shown to be modulated by the lncRNA Sros1, which blocks the dimerization of CAPRIN1 and indirectly reduces the half-life of Stat1 mRNA (*30*). A notable feature of these studies is the ability of ncRNAs to affect gene expression through CAPRIN1, albeit in different ways. In contrast to Sros1, GIRGL enhances CAPRIN1 dimerization, and thus, its effects on GLS1 expression appear more consistent with the actions of the dengue-derived ncRNAs that antagonize target gene translation as part of a larger ribonucleoprotein (RNP) complex. The region of

GIRGL involved in CAPRIN1 binding is a predicted symmetrical Y shape, and given that both arms were necessary to support CAPRIN1 dimerization, this suggests that these arms act tandemly to promote CAPRIN1 dimerization.

CAPRIN1 and G3BP1 are regulatory components of the membraneless RNP organelles called SGs (*36*). The composition of the GIRGL-RNP complex involving CAPRIN1 and G3BP1 is itself instructive given previous examples (*36*, *44*). SGs represent cytoplasmic condensates of RNPs that arise in response to different environmental insults including heat shock, hypoxia, hyperosmolarity, oxidative stress, and nutrient starvation along with pathological conditions such as viral infection (*32*). SGs form dynamically by liquid-liquid phase separation and are thought to represent stalled initiation complexes resulting from polysome disassembly (*54*–*56*). In toto, our experimental observations strongly suggest that GIRGL regulates GLS1 translation via SGs.

Metabolic stress caused by glutamine deficiency up-regulates GIRGL, and this coincides with the formation of SGs containing CAPRIN1, GLS1 mRNA, and GIRGL. In the absence of stress, forced expression of GIRGL resulted in the formation of CAPRIN1-based SGs, recapitulating the phenomenon typically observed when SG components are overexpressed (*46*). Complexes of CAPRIN1, GLS1 mRNA, and GIRGL were shown to exist in cells and can form in vitro, where specific binding regions were mapped between CAPRIN1, GIRGL, and GLS1 mRNA. In particular, CAPRIN1 bound to the 3′UTR of GLS1 mRNA through its highly conserved RGG domain, which is consistent with interactions between other target mRNAs such as c-MYC and cyclin D2 that undergo entry into SGs (*31*). Furthermore, within cells, GIRGL negatively affected the inclusion on GLS1 mRNA in ribosomal and polyribosomal containing fractions, indicating how it affects GLS1 translation. Crucially, it was shown that the inclusion of GIRGL promotes the efficiency of phase separation of CAPRIN1-GLS1, the fundamental basis of SG formation. It seems probable that the ability of GIRGL to facilitate CAPRIN1 dimerization is an initiating feature of this process.

From a broader perspective, SGs are not the only type of RNP-based condensates to exist within cells (*57*). In addition to SGs, there are also cytoplasmic P-bodies and neuronal granules together with nuclear suborganelles including the nucleolus and nuclear paraspeckles. While progress is being made into how RNP condensates form (*58*), another equally important aspect to consider is how their composition and function are regulated to deal with specific stressors. Certain RNA chaperones may be specifically associated with either SGs or P-bodies, while some are found associated with both (*57*). Here, we found that CAPRIN1, but not G3BP1, was required to allow cells to specifically respond. Glutamine deprivation stress resulted in the compartmentalization and translational inhibition of GLS1 mRNA, the key enzyme involved in the catabolism of the depleted substrate. Moreover, while the lncRNA NEAT1 is known to be an essential structural component of nuclear paraspeckles (*59*), to our best knowledge, this is the first reported lncRNA implicated in SG formation.

Following on from this is the general interest in the role of RNP condensates in disease states. Here, we considered the impact of GIRGL on tumorigenesis, showing that GIRGL was strongly up-regulated in response to glutamine deprivation in colon cancer lines, but not in normal NCM460 colorectal cells. Moreover, the growth of colon cancer cells under glutamine-replete conditions was negatively affected by GIRGL expression both in vitro and in vivo, consistent with its effects on GLS1 expression. However, GIRGL expression was shown to positively affect cancer cell survival following prolonged glutamine deprivation, indicating a role during nutrient stress. Because GIRGL inhibits GLS1 expression under such conditions, we speculate that this acts as a preservative measure used to dampen the consumption of the limited glutamine resource, which, in turn, favors cell survival. Glutamine levels can become limiting within the solid tumor microenvironment, and likely reflecting its activation in vivo, the expression of GIRGL was increased in a subset of colon cancers. However, whether this mechanism of cellular adaptation affects disease outcomes remains to be determined along with the role of GIRGL in other pathophysiological contexts.

MATERIALS AND METHODS

Reagents, antibodies, and recombinant DNA

Reagents are shown in table S4.1, antibodies are shown in table S4.2, and recombinant DNA is shown in table S5.

Cell culture and lentiviral transduction

HCT116, HT29, and human embryonic kidney (HEK) 293T cells were cultured in Dulbecco's modified Eagle's medium containing 10% fetal bovine serum and 1% sodium pyruvate and maintained at 37°C in 5% CO_2, whereas the NCM460 cell line was cultured in RPMI 1640 (Gibco). Lentiviruses for gene knockdown and overexpression experiments were generated by transfecting HEK293T cells for 48 hours with pLKO.1–based shRNAs, pRev, pGag, and pVSVG (2:2:2:1 ratio) or pSIN/pCDH, psPAX2, and pMD2.G (2:2:1 ratio). Supernatants were 0.45 μm–filtered, supplemented with polybrene (8 μg/ml) (Sigma-Aldrich) before incubating with target cells and selecting with puromycin (1 mg/ml). Targeting sequences are shown in table S3.2.

Quantitative and semiquantitative PCR

Total RNA isolated using TRIzol reagent (Invitrogen) was used to synthesize complementary DNA (cDNA) using the Prime-Script RT Reagent Kit (Takara). qPCR assays were performed using SYBR Green real-time PCR analysis (Takara) with the specified primers (table S3.1), and the results were recorded as cycle thresholds (C_t) normalized against the internal control (β-actin). Alternatively, semiquantitative PCR was performed using 2× Taq PCR mix with 25 cycles for internal controls and 30 to 40 cycles for lncRNAs.

Absolute RNA quantitation

Standard curve assays were used, where absolute quantitation of RNA expression was required. Plasmids containing the target cDNA of interest were used to construct standard curves by plotting C_t values against copy number as determined from the adjusted final concentration of plasmids. RNA was extracted from a fixed number of cells and cDNA equivalents from 2000 cells used in each qPCR. Average RNA copy numbers per cell were calculated from the sample C_t values referenced against the linear portion of the standard curve.

Metabolic measurements

Cellular glutamine consumption, glutaminase activity, α-KG, α-KGDH, ATP, NADPH/$NADP^+$ ratio, GSH [glutathione (reduced form)], ROS, glutamate, aspartate, and asparagine levels were measured using the glutamine assay (BioAssay Systems), glutaminase activity assay (BioVision), α-KG assay (BioVision), α-KGDH assay (BioVision), ATP assay (BioVision), NADPH/$NADP^+$ ratio assay (BioVision), total GSH assay (Sigma-Aldrich) kits, ROS assay (Thermo Fisher

Scientific), glutamate assay (BioAssay Systems), aspartate assay (Abcam) and asparagine assay (Abcam), respectively, according to the manufacturer's instructions.

DNA, RNA, and protein synthesis assays

To measure DNA synthesis, cells were cultured with or without 2 mM glutamine in the presence of 5-EdU (5-ethynyl-2′deoxyuridine) for 24 hours (DNA synthesis assay kit, BioVision). Results were assessed using epifluorescence microscopy to reveal de novo synthesis as EdU incorporation [red fluorescent protein (RFP) filter, red] versus total DNA (GFP filter, green). Alternatively, RNA synthesis levels were measured using RNA synthesis assay kit (Abcam). After culture with or without 2 mM glutamine for 24 hours, cells were pulsed for 2 hours with 5-EU (ethynyl uridine) and RNA incorporation measured by fluorescence (excitation/emission) = 494/521 nm), normalizing values to total RNA. Protein synthesis levels were measured using a protein synthesis assay kit (BioVision) by pulsing cells for 2 hours with *O*-propargyl-puromycin, and protein incorporation was measured by fluorescence (excitation/emission = 494/521 nm), normalizing values to total protein.

GFP reconstitution assay

The predicted IRES of GIRGL (1 to 175 bp) was inserted into the pCirc-GFP-IRES circular RNA (circRNA) translation reporter containing a split GFP system using Eco RI and Eco RV (*37*).

Oxygen consumption rate

Seahorse XFe24 analyzer (Seahorse Bioscience, Agilent) assays were performed according to the manufacturer's instructions. Briefly, 3×10^4 to 5×10^4 cells per well were seeded in 24-well XF cell culture microplates in growth medium for 24 hours before changing the medium to XF base medium (pH 7.4) containing pyruvate (1 mM), glutamine (1 mM), and glucose (10 mM). After 1-hour equilibration, oligomycin (1.5 mM), FCCP (carbonyl cyanide *p*-trifluoromethoxyphenylhydrazone) (0.5 mM), and rotenone/antimycin A (0.5 mM) were sequentially added, with data analyzed using the Seahorse XF Glycolysis Stress Test Report Generator package.

In vitro transcription and RNA pull-down assays

In vitro transcription reactions were performed as previously described (*60*) using primer sequences appended to table S3.5. For the RNA pull-down assays, cell lysates prepared by ultrasonication in RIP buffer were precleared against streptavidin-coated magnetic beads (Invitrogen). In vitro transcribed biotin-labeled RNA or DNA probes (table S3.4) adsorbed to the streptavidin beads were then incubated with cell lysates at 4°C for 4 hours before washing five times in RIP buffer and elution in Laemmli sample buffer.

RNA in situ hybridization and immunofluorescence

Cells were fixed on glass coverslips in 4% formaldehyde and permeabilized using 0.1% Triton X-100 before performing RNA in situ hybridization reactions as previously described (*60*). In vitro transcribed probes were prepared as described above (probe sequence shown in table S3.6) and Alexa Fluor–labeled using the Nucleic Acid Labeling Kit (Invitrogen). Cell nuclei were counterstained by 4′,6-diamidino-2-phenylindole (DAPI), and images were acquired using a Leica TCS SP8 confocal system. For immunofluorescence (IF) staining, cells were prepared as for FISH, then blocked with 5% bovine serum albumin, and incubated for 1 hour at room temperature with primary antibodies before addition of Alexa Fluor secondary antibodies for 0.5 hour at room temperature. For combination FISH/IF staining, FISH was conducted first before IF staining.

Western blotting and IPs

Western blots were performed as previously described (*60*). For IPs, cells were lysed in IP lysis buffer [150 mM NaCl, 50 mM tris (pH 7.4), 10% glycerol, and 1.5 mM $MgCl_2$] supplemented with protease inhibitor phenylmethylsulfonyl fluoride and cocktail before incubation for 4 hours at 4°C with protein A/G beads precoated with indicated antibodies. Beads were washed three times using IP lysis buffer and eluted (95°C, 10 min), and the samples were analyzed by Western blotting. Steps were performed under ribonuclease (RNase)–free conditions as required. Alternatively, cell lysates were prepared for two-step IPs using lysis buffer containing 20 mM Hepes (pH 7.8), 400 mM KCl, 5% glycerol, 5 mM EDTA, 1% NP-40, protease inhibitor cocktail, and RNase inhibitor. The first IP used anti-Flag antibodies before elution with Flag peptides. Ten percent of the sample was reserved for Western blotting and semiquantitative reverse transcription PCR (RT-PCR) analysis, while the remaining eluate was subjected to the secondary IP.

RNA immunoprecipitation

RIP assays were performed as described (*61*). Briefly, cells were lysed in RIP buffer [150 mM KCl, 25 mM tris (pH 7.4), 0.5 mM dithiothreitol (DTT), 0.5% NP-40, protease inhibitor cocktail (Roche), and RNase inhibitors]. Soluble cell lysates were precleared with protein A/G beads alone before IP with the indicated antibodies at 4°C for 3 hours. After washing, the bead-bound immunocomplexes were eluted using elution buffer [50 mM tris (pH 8.0), 1% SDS, and 10 mM EDTA] at 65°C for 10 min. To isolate protein-associated RNAs from the eluted immunocomplexes, samples were treated with proteinase K, and RNAs were extracted by phenol/chloroform before RT-PCR analysis.

Chromatin IP

ChIP assays were performed according to the manufacturer's instructions (Cell Signaling Technology). Bound DNA fragments were subjected to quantitative or semiquantitative PCR using specific primers (table S3.3). Primers amplifying target sequences in the MMP1 and glyceraldehyde-3-phosphate dehydrogenase (GAPDH) promoters were used as positive and negative controls, respectively.

Luciferase reporter assay

Assays were performed as previously described (*61*) using the Dual-Luciferase Reporter Assay System (Promega).

Polysome profiling

Polysome profiling assays were performed as described previously using cells seeded in 15-cm dishes (*62*). After indicated treatments, cells were pulsed with cycloheximide (100 μg/ml) for 10 min, washed in ice-cold phosphate-buffered saline containing cycloheximide (100 ug/ml), and lysed in polysome lysis buffer [5 mM tris-HCl (pH 7.5), 2.5 mM $MgCl_2$, 1.5 mM KCl, 1 mM DTT, 0.5% Triton X-100, 0.5% sodium deoxycholate, cycloheximide (100 μg/ml), 100 U of ribonuclease (RNase) inhibitor, and EDTA-free protease inhibitor]. Clarified lysates were then layered onto 11 ml of 10 to 45% sucrose density gradients [20 mM Hepes-KOH, 5 mM $MgCl_2$, 100 mM KCl, 1 mM DTT, cycloheximide (100 mg/ml), and 10 to 45%

RNase-free sucrose] and centrifuged in an SW-41Ti rotor at 40,000 rpm at 4°C for 2 hours. Fractions were acquired using the Labconco Auto Densi-Flow Gradient Fractionator connected to an Isco Tris pump with constant monitoring of optical density (OD) at 254 nm. Total RNA was extracted from each fraction using TRIzol, and cDNA prepared using the SuperScript III reverse transcriptase (Invitrogen) with transcript abundance was determined by qPCR.

Subcellular fractionation

Subcellular fractionation was performed as previously described (*60*).

Phase separation assays

Phase separation assays were performed as described previously (*46*, *63*). Briefly, the indicated recombinant proteins were prepared in buffer [25 mM Na_2HPO_4 (pH 7.4), 30 mM NaCl, and 2 mM DTT] before mixing with in vitro transcribed Alexa Fluor–labeled RNAs diluted in tris-EDTA buffer. Protein-RNA solutions were thoroughly mixed and incubated at room temperature, following which 10 μl of the mixture was transferred onto a 35-mm glass-bottom dish (NEST 801001) and immediately imaged. Confocal fluorescence images were obtained using a Leica TCS SP8 confocal system. The presence or absence of droplet formation in different conditions (phase separation) was determined by round droplets with greater or equal to 1 μm diameter. All images represent a single focal plane focused onto the surface of the glass slide. Phase separation was quantified as the index of dispersion ($\sigma 2/\mu$), where the variance in the fluorescence intensity per image was determined and normalized to the mean fluorescence intensity of the solution phase. At least 20 randomly selected regions (36 × 36 μm each) were analyzed for each condition to achieve a representative sample measure. Each datum point presented in the bar graphs was derived from one imaging region. Accompanying analyses of protein and RNA in the dilute and condensed phases were performed as described previously (*63*–*64*).

Fluorescence recovery after photobleaching

FRAP assays were conducted using the FRAP module of the Leica TCS SP8 confocal system. Circular regions of interest were software-defined in the phase separation droplets and bleached using 95% laser power with either the 488- or 561-nm laser lines as required. Time-lapse images were collected, and fluorescence recovery was quantified as described in (*63*, *65*).

Xenograft model

Balb/c nude mice (4 weeks old, ♂), obtained from Beijing Vital River Laboratory Animal Technology Co. Ltd., were maintained in a specific pathogen–free facility. Studies on animals were conducted with approval from the Animal Research Ethics Committee of Zhengzhou University.

Quantification and statistical analyses

No statistical methods were used to predetermine sample size. Statistical analysis was carried out using Microsoft Excel and GraphPad Prism 8 to assess differences between experimental groups. Densitometry was performed where indicated using Image Lab software. Statistical significance was analyzed by two-tailed Student's *t* test for comparisons of two samples. Tests performed with $P < 0.05$ were considered statistically significant (ns, not significant, $^{*}P < 0.05$, $^{**}P < 0.01$, $^{***}P < 0.001$).

SUPPLEMENTARY MATERIALS

Supplementary material for this article is available at http://advances.sciencemag.org/cgi/content/full/7/13/eabe5708/DC1

View/request a protocol for this paper from *Bio-protocol*.

REFERENCES AND NOTES

1. J. R. Mayers, M. G. Vander Heiden, Famine versus feast: Understanding the metabolism of tumors in vivo. *Trends Biochem. Sci.* **40**, 130–140 (2015).
2. J. Bergström, P. Fürst, L. O. Norée, E. Vinnars, Intracellular free amino acid concentration in human muscle tissue. *J. Appl. Physiol.* **36**, 693–697 (1974).
3. R. J. DeBerardinis, T. Cheng, Q's next: The diverse functions of glutamine in metabolism, cell biology and cancer. *Oncogene* **29**, 313–324 (2010).
4. M. Yuneva, N. Zamboni, P. Oefner, R. Sachidanandam, Y. Lazebnik, Deficiency in glutamine but not glucose induces MYC-dependent apoptosis in human cells. *J. Cell Biol.* **178**, 93–105 (2007).
5. M. C. Kerr, R. D. Teasdale, Defining macropinocytosis. *Traffic* **10**, 364–371 (2009).
6. Y. D. Bhutia, E. Babu, S. Ramachandran, V. Ganapathy, Amino Acid transporters in cancer and their relevance to "glutamine addiction": Novel targets for the design of a new class of anticancer drugs. *Cancer Res.* **75**, 1782–1788 (2015).
7. B. J. Altman, Z. E. Stine, C. V. Dang, From Krebs to Clinic: Glutamine metabolism to cancer therapy. *Nat. Rev. Cancer* **16**, 619–634 (2016).
8. T. C. Welbourne, Ammonia production and glutamine incorporation into glutathione in the functioning rat kidney. *Can. J. Biochem.* **57**, 233–237 (1979).
9. D. Botman, W. Tigchelaar, C. J. F. Van Noorden, Determination of glutamate dehydrogenase activity and its kinetics in mouse tissues using metabolic mapping (quantitative enzyme histochemistry). *J. Histochem. Cytochem.* **62**, 802–812 (2014).
10. N. P. Curthoys, M. Watford, Regulation of glutaminase activity and glutamine metabolism. *Annu. Rev. Nutr.* **15**, 133–159 (1995).
11. GTEx Consortium, The Genotype-Tissue Expression (GTEx) pilot analysis: Multitissue gene regulation in humans. *Science* **348**, 648–660 (2015).
12. P. Gao, I. Tchernyshyov, T.-C. Chang, Y.-S. Lee, K. Kita, T. Ochi, K. I. Zeller, A. M. De Marzo, J. E. Van Eyk, J. T. Mendell, C. V. Dang, c-Myc suppression of miR-23a/b enhances mitochondrial glutaminase expression and glutamine metabolism. *Nature* **458**, 762–765 (2009).
13. J.-B. Wang, J. W. Erickson, R. Fuji, S. Ramachandran, P. Gao, R. Dinavahi, K. F. Wilson, A. L. B. Ambrosio, S. M. G. Dias, C. V. Dang, R. A. Cerione, Targeting mitochondrial glutaminase activity inhibits oncogenic transformation. *Cancer Cell* **18**, 207–219 (2010).
14. S. Suzuki, T. Tanaka, M. V. Poyurovsky, H. Nagano, T. Mayama, S. Ohkubo, M. Lokshin, H. Hosokawa, T. Nakayama, Y. Suzuki, S. Sugano, E. Sato, T. Nagao, K. Yokote, I. Tatsuno, C. Prives, Phosphate-activated glutaminase (GLS2), a p53-inducible regulator of glutamine metabolism and reactive oxygen species. *Proc. Natl. Acad. Sci. U.S.A.* **107**, 7461–7466 (2010).
15. J. Zhang, C. Wang, M. Chen, J. Cao, Y. Zhong, L. Chen, H.-M. Shen, D. Xia, Epigenetic silencing of glutaminase 2 in human liver and colon cancers. *BMC Cancer* **13**, 601 (2013).
16. A. Cassago, A. P. S. Ferreira, I. M. Ferreira, C. Fornezari, E. R. M. Gomes, K. S. Greene, H. M. Pereira, R. C. Garratt, S. M. G. Dias, A. L. B. Ambrosio, Mitochondrial localization and structure-based phosphate activation mechanism of glutaminase C with implications for cancer metabolism. *Proc. Natl. Acad. Sci. U.S.A.* **109**, 1092–1097 (2012).
17. R. A. Shapiro, L. Farrell, M. Srinivasan, N. P. Curthoys, Isolation, characterization, and in vitro expression of a cDNA that encodes the kidney isoenzyme of the mitochondrial glutaminase. *J. Biol. Chem.* **266**, 18792–18796 (1991).
18. L. Sun, L. Song, Q. Wan, G. Wu, X. Li, Y. Wang, J. Wang, Z. Liu, X. Zhong, X. He, S. Shen, X. Pan, A. Li, Y. Wang, P. Gao, H. Tang, H. Zhang, cMyc-mediated activation of serine biosynthesis pathway is critical for cancer progression under nutrient deprivation conditions. *Cell Res.* **25**, 429–444 (2015).
19. J. J. Quinn, H. Y. Chang, Unique features of long non-coding RNA biogenesis and function. *Nat. Rev. Genet.* **17**, 47–62 (2016).
20. J. E. Wilusz, H. Sunwoo, D. L. Spector, Long noncoding RNAs: Functional surprises from the RNA world. *Genes Dev.* **23**, 1494–1504 (2009).
21. W. L. Hu, L. Jin, A. Xu, Y. F. Wang, R. F. Thorne, X. D. Zhang, M. Wu, GUARDIN is a p53-responsive long non-coding RNA that is essential for genomic stability. *Nat. Cell Biol.* **20**, 492–502 (2018).
22. A. Sanchez Calle, Y. Kawamura, Y. Yamamoto, F. Takeshita, T. Ochiya, Emerging roles of long non-coding RNA in cancer. *Cancer Sci.* **109**, 2093–2100 (2018).
23. P. Wang, J. Xu, Y. Wang, X. Cao, An interferon-independent lncRNA promotes viral replication by modulating cellular metabolism. *Science* **358**, 1051–1055 (2017).
24. S.-J. Deng, H.-Y. Chen, Z. Zeng, S. Deng, S. Zhu, Z. Ye, C. He, M.-L. Liu, K. Huang, J.-X. Zhong, F.-Y. Xu, Q. Li, Y. Liu, C. Wang, G. Zhao, Nutrient stress–dysregulated antisense lncRNA GLS-AS impairs GLS-mediated metabolism and represses pancreatic cancer progression. *Cancer Res.* **79**, 1398–1412 (2019).
25. R. S. Redis, L. E. Vela, W. Lu, J. F. de Oliveira, C. Ivan, C. Rodriguez-Aguayo, D. Adamoski, B. Pasculli, A. Taguchi, Y. Chen, A. F. Fernandez, L. Valledor, K. Van Roosbroeck, S. Chang,

M. Shah, G. Kinnebrew, L. Han, Y. Atlasi, L. H. Cheung, G. Y. Huang, P. Monroig, M. S. Ramirez, T. C. Ivkovic, L. Van, H. Ling, R. Gafà, S. Kapitanovic, G. Lanza, J. A. Bankson, P. Huang, S. Y. Lai, R. C. Bast, M. G. Rosenblum, M. Radovich, M. Ivan, G. Bartholomeusz, H. Liang, M. F. Fraga, W. R. Widger, S. Hanash, I. Berindan-Neagoe, G. Lopez-Berestein, A. L. B. Ambrosio, S. M. G. Dias, G. A. Calin, Allele-specific reprogramming of cancer metabolism by the long non-coding RNA CCAT2. *Mol. Cell* **61**, 520–534 (2016).
26. X. Wang, R. Liu, W. Zhu, H. Chu, H. Yu, P. Wei, X. Wu, H. Zhu, H. Gao, J. Liang, G. Li, W. Yang, UDP-glucose accelerates *SNAI1* mRNA decay and impairs lung cancer metastasis. *Nature* **571**, 127–131 (2019).
27. K. Abdelmohsen, M. Gorospe, Posttranscriptional regulation of cancer traits by HuR. *WIREs RNA* **1**, 214–229 (2010).
28. H. H. Kim, Y. Kuwano, S. Srikantan, E. K. Lee, J. L. Martindale, M. Gorospe, HuR recruits let-7/RISC to repress c-Myc expression. *Genes Dev.* **23**, 1743–1748 (2009).
29. J.-H. Yoon, K. Abdelmohsen, S. Srikantan, X. Yang, J. L. Martindale, S. De, M. Huarte, M. Zhan, K. G. Becker, M. Gorospe, LincRNA-p21 suppresses target mRNA translation. *Mol. Cell* **47**, 648–655 (2012).
30. H. Xu, Y. Jiang, X. Xu, X. Su, Y. Liu, Y. Ma, Y. Zhao, Z. Shen, B. Huang, X. Cao, Inducible degradation of lncRNA Sros1 promotes IFN-γ-mediated activation of innate immune responses by stabilizing *Stat1* mRNA. *Nat. Immunol.* **20**, 1621–1630 (2019).
31. S. Solomon, Y. Xu, B. Wang, M. D. David, P. Schubert, D. Kennedy, J. W. Schrader, Distinct structural features of caprin-1 mediate its interaction with G3BP-1 and its induction of phosphorylation of eukaryotic translation initiation factor 2α, entry to cytoplasmic stress granules, and selective interaction with a subset of mRNAs. *Mol. Cell. Biol.* **27**, 2324–2342 (2007).
32. H. Katoh, T. Okamoto, T. Fukuhara, H. Kambara, E. Morita, Y. Mori, W. Kamitani, Y. Matsuura, Japanese encephalitis virus core protein inhibits stress granule formation through an interaction with caprin-1 and facilitates viral propagation. *J. Virol.* **87**, 489–502 (2013).
33. K. Nakayama, R. Ohashi, Y. Shinoda, M. Yamazaki, M. Abe, A. Fujikawa, S. Shigenobu, A. Futatsugi, M. Noda, K. Mikoshiba, T. Furuichi, K. Sakimura, N. Shiina, RNG105/caprin1, an RNA granule protein for dendritic mRNA localization, is essential for long-term memory formation. *eLife* **6**, e29677 (2017).
34. T. H. Kim, B. Tsang, R. M. Vernon, N. Sonenberg, L. E. Kay, J. D. Forman-Kay, Phospho-dependent phase separation of FMRP and CAPRIN1 recapitulates regulation of translation and deadenylation. *Science* **365**, 825–829 (2019).
35. K. Bidet, D. Dadlani, M. A. Garcia-Blanco, G3BP1, G3BP2 and CAPRIN1 are required for translation of interferon stimulated mRNAs and are targeted by a dengue virus non-coding RNA. *PLOS Pathog.* **10**, e1004242 (2014).
36. N. Kedersha, M. D. Panas, C. A. Achorn, S. Lyons, S. Tisdale, T. Hickman, M. Thomas, J. Lieberman, G. M. McInerney, P. Ivanov, P. Anderson, G3BP-Caprin1-USP10 complexes mediate stress granule condensation and associate with 40S subunits. *J. Cell Biol.* **212**, 845–860 (2016).
37. Y. Yang, X. Fan, M. Mao, X. Song, P. Wu, Y. Zhang, Y. Jin, Y. Yang, L.-L. Chen, Y. Wang, C. C. Wong, X. Xiao, Z. Wang, Extensive translation of circular RNAs driven by N^6-methyladenosine. *Cell Res.* **27**, 626–641 (2017).
38. J. Zhang, J. Fan, S. Venneti, J. R. Cross, T. Takagi, B. Bhinder, H. Djaballah, M. Kanai, E. H. Cheng, A. R. Judkins, B. Pawel, J. Baggs, S. Cherry, J. D. Rabinowitz, C. B. Thompson, Asparagine plays a critical role in regulating cellular adaptation to glutamine depletion. *Mol. Cell* **56**, 205–218 (2014).
39. S. X. Xiang, H. Gu, L. Jin, R. F. Thorne, X. D. Zhang, M. Wu, LncRNA IDH1-AS1 links the functions of c-Myc and HIF1α via IDH1 to regulate the Warburg effect. *Proc. Natl. Acad. Sci. U.S.A.* **115**, E1465–E1474 (2018).
40. S. L. Colombo, M. Palacios-Callender, N. Frakich, S. Carcamo, I. Kovacs, S. Tudzarova, S. Moncada, Molecular basis for the differential use of glucose and glutamine in cell proliferation as revealed by synchronized HeLa cells. *Proc. Natl. Acad. Sci. U.S.A.* **108**, 21069–21074 (2011).
41. H. Matsuki, M. Takahashi, M. Higuchi, G. N. Makokha, M. Oie, M. Fujii, Both G3BP1 and G3BP2 contribute to stress granule formation. *Genes Cells* **18**, 135–146 (2013).
42. I. Passacantilli, P. Frisone, E. De Paola, M. Fidaleo, M. P. Paronetto, hnRNPM guides an alternative splicing program in response to inhibition of the PI3K/AKT/mTOR pathway in Ewing sarcoma cells. *Nucleic Acids Res.* **45**, 12270–12284 (2017).
43. T.-M. Chen, M.-C. Lai, Y.-H. Li, Y.-L. Chan, C.-H. Wu, Y.-M. Wang, C.-W. Chien, S.-Y. Huang, H. S. Sun, S.-J. Tsai, hnRNPM induces translation switch under hypoxia to promote colon cancer development. *EBioMedicine* **41**, 299–309 (2019).
44. Y. Wu, J. Zhu, X. Huang, Z. Du, Crystal structure of a dimerization domain of human Caprin-1: Insights into the assembly of an evolutionarily conserved ribonucleoprotein complex consisting of Caprin-1, FMRP and G3BP1. *Acta Crystallogr. D Struct. Biol.* **72**, 718–727 (2016).
45. S. Alberti, Phase separation in biology. *Curr. Biol.* **27**, R1097–R1102 (2017).
46. B. Tsang, J. Arsenault, R. M. Vernon, H. Lin, N. Sonenberg, L.-Y. Wang, A. Bah, J. D. Forman-Kay, Phosphoregulated FMRP phase separation models activity-dependent translation through bidirectional control of mRNA granule formation. *Proc. Natl. Acad. Sci. U.S.A.* **116**, 4218–4227 (2019).
47. V. Gouirand, F. Guillaumond, S. Vasseur, Influence of the tumor microenvironment on cancer cells metabolic reprogramming. *Front. Oncol.* **8**, 117 (2018).
48. C. Carmona-Fontaine, M. Deforet, L. Akkari, C. B. Thompson, J. A. Joyce, J. B. Xavier, Metabolic origins of spatial organization in the tumor microenvironment. *Proc. Natl. Acad. Sci. U.S.A.* **114**, 2934–2939 (2017).
49. M. Tajan, A. K. Hock, J. Blagih, N. A. Robertson, C. F. Labuschagne, F. Kruiswijk, T. J. Humpton, P. D. Adams, K. H. Vousden, A role for p53 in the adaptation to glutamine starvation through the expression of SLC1A3. *Cell Metab.* **28**, 721–736.e6 (2018).
50. X. H. Lowman, E. A. Hanse, Y. Yang, M. B. Ishak Gabra, T. Q. Tran, H. Li, M. Kong, p53 promotes cancer cell adaptation to glutamine deprivation by upregulating Slc7a3 to increase arginine uptake. *Cell Rep.* **26**, 3051–3060.e4 (2019).
51. H. Rubin, Deprivation of glutamine in cell culture reveals its potential for treating cancer. *Proc. Natl. Acad. Sci. U.S.A.* **116**, 6964–6968 (2019).
52. N. P. Shanware, K. Bray, C. H. Eng, F. Wang, M. Follettie, J. Myers, V. R. Fantin, R. T. Abraham, Glutamine deprivation stimulates mTOR-JNK-dependent chemokine secretion. *Nat. Commun.* **5**, 4900 (2014).
53. M. A. Bogoyevitch, B. Kobe, Uses for JNK: The many and varied substrates of the c-Jun N-terminal kinases. *Microbiol. Mol. Biol. Rev.* **70**, 1061–1095 (2006).
54. S. F. Banani, H. O. Lee, A. A. Hyman, M. K. Rosen, Biomolecular condensates: Organizers of cellular biochemistry. *Nat. Rev. Mol. Cell Biol.* **18**, 285–298 (2017).
55. Y. Shin, C. P. Brangwynne, Liquid phase condensation in cell physiology and disease. *Science* **357**, eaaf4382 (2017).
56. A. A. Deniz, Networking and dynamic switches in biological condensates. *Cell* **181**, 228–230 (2020).
57. D. Tauber, G. Tauber, R. Parker, Mechanisms and regulation of RNA condensation in RNP granule formation. *Trends Biochem. Sci.* **45**, 764–778 (2020).
58. J. Guillén-Boixet, A. Kopach, A. S. Holehouse, S. Wittmann, M. Jahnel, R. Schlüßler, K. Kim, I. R. E. A. Trussina, J. Wang, D. Mateju, I. Poser, S. Maharana, M. Ruer-Gruß, D. Richter, X. Zhang, Y.-T. Chang, J. Guck, A. Honigmann, J. Mahamid, A. A. Hyman, R. V. Pappu, S. Alberti, T. M. Franzmann, RNA-induced conformational switching and clustering of G3BP drive stress granule assembly by condensation. *Cell* **181**, 346–361.e17 (2020).
59. C. M. Clemson, J. N. Hutchinson, S. A. Sara, A. W. Ensminger, A. H. Fox, A. Chess, J. B. Lawrence, An architectural role for a nuclear non-coding RNA: NEAT1 RNA is essential for the structure of paraspeckles. *Mol. Cell* **33**, 717–726 (2009).
60. Q. Li, Y. Wang, S. Wu, Z. Zhou, X. Ding, R. Shi, R. F. Thorne, X. D. Zhang, W. Hu, M. Wu, CircACC1 regulates assembly and activation of AMPK complex under metabolic stress. *Cell Metab.* **30**, 157–173.e7 (2019).
61. F. Yang, H. F. Zhang, Y. D. Mei, M. Wu, Reciprocal regulation of HIF-1α and lincRNA-p21 modulates the Warburg effect. *Mol. Cell* **53**, 88–100 (2014).
62. L. Li, Y. Mao, L. Zhao, L. Li, J. Wu, M. Zhao, W. Du, L. Yu, P. Jiang, p53 regulation of ammonia metabolism through urea cycle controls polyamine biosynthesis. *Nature* **567**, 253–256 (2019).
63. A. Jain, R. D. Vale, RNA phase transitions in repeat expansion disorders. *Nature* **546**, 243–247 (2017).
64. G. Zhu, J. Xie, W. Kong, J. Xie, Y. Li, L. Du, Q. Zheng, L. Sun, M. Guan, H. Li, T. Zhu, H. He, Z. Liu, X. Xia, C. Kan, Y. Tao, H. C. Shen, D. Li, S. Wang, Y. Yu, Z.-H. Yu, Z.-Y. Zhang, C. Liu, J. Zhu, Phase separation of disease-associated SHP2 mutants underlies MAPK hyperactivation. *Cell* **183**, 490–502.e18 (2020).
65. M. R. White, D. M. Mitrea, P. Zhang, C. B. Stanley, D. E. Cassidy, A. Nourse, A. H. Phillips, M. Tolbert, J. P. Taylor, R. W. Kriwacki, C9orf72 Poly (PR) dipeptide repeats disturb biomolecular phase separation and disrupt nucleolar function. *Mol. Cell* **74**, 713–728.e6 (2019).

Acknowledgments: We thank P. Jiang and Y. Mao (Tsinghua University, Beijing, China) for technical support. We also thank W. Hu (Zhengzhou University, Zhengzhou, China) for providing NCM460 cell line. **Funding:** This work was funded by the National Key R&D Program of China (2018YFA0107100), the National Natural Science Foundation of China (81820108021, 31871437, and 81773815), and NHMRC Australia (1147271). **Author contributions:** R.W., L.C., F.S., L.Z., and M.W. designed the research. R.W. and L.C. performed most of the experiments. R.W., L.C., R.F.T., X.D.Z., J.L., and M.W. carried out data analysis. R.F.T., M.W., and R.W. wrote the manuscript. **Competing interests:** The authors declare that they have no competing interests. **Data and materials availability:** All data needed to evaluate the conclusions in the paper are present in the paper and/or the Supplementary Materials. Additional data related to this paper may be requested from the authors.

Submitted 31 August 2020
Accepted 4 February 2021
Published 24 March 2021
10.1126/sciadv.abe5708

Citation: R. Wang, L. Cao, R. F. Thorne, X. D. Zhang, J. Li, F. Shao, L. Zhang, M. Wu, LncRNA GIRGL drives CAPRIN1-mediated phase separation to suppress glutaminase-1 translation under glutamine deprivation. *Sci. Adv.* **7**, eabe5708 (2021).